**FUNCTIONAL PRIONS IN MAMMALIAN INNATE IMMUNE SIGNALING**

APPROVED BY SUPERVISORY COMMITTEE

Zhijian J. Chen, Ph.D (Supervisor)

Bruce Beutler, MD

Joseph L. Goldstein, MD

Andrew R. Zinn, MD/Ph.D (Chair)

DEDICATION

**TO THOSE WHO INSPIRE ME, MY FAMILY, FRIENDS, AND COLLEAGUES**

ACKNOWLEDGEMENTS

**I'm extremely grateful to my mentor Dr. James Chen for his generous support, patience, and guidance. Most importantly, he taught me that science is a lifestyle, and the only way to be truly satisfied is to do great work. And the only way to do great work is to love what you do.**

**I'm eternally indebted to Siqi Liu for her unwavering care and support. She and I are a team and I wouldn't be here without her.**

**To my collaborators (especially Randal Halfmann) and colleagues, thank you for being a part of this incredible journey. It's been an honor working with you.**

**To my family and friends, thanks for your inspiration.**

# FUNCTIONAL PRIONS IN MAMMALIAN INNATE IMMUNE SIGNALING

by

XIN CAI

DISSERTATION THESIS

Presented to the Faculty of the Graduate School of Biomedical Sciences

The University of Texas Southwestern Medical Center at Dallas

In Partial Fulfillment of the Requirements

For the Degree of

DOCTOR OF PHILOSOPHY

The University of Texas Southwestern Medical Center at Dallas

Dallas, Texas

June, 2014

**FUNCTIONAL PRIONS IN MAMMALIAN INNATE IMMUNE SIGNALING**

Publication No. _____

Xin Cai, Ph.D

The University of Texas Southwestern Medical Center at Dallas, 2014

Supervising Professor: Zhijian James Chen, Ph.D

Pathogens and cellular danger signals activate mammalian cytosolic sensors such as RIG-I and NLRP3 which signal through respective adaptor proteins MAVS and ASC to produce robust innate immune and inflammatory responses. MAVS and ASC harbor N-terminal CARD and PYRIN domains, respectively, essential for their signaling ability. Using the Sup35 based yeast prion assay, we show that CARD and PYRIN function as bona fide prions in yeast when fused to Sup35C. In response to respective upstream sensors RIG-I and NLRP3, both CARD and PYRIN form self-perpetuating, SDS-resistant polymers that are inherited cytoplasmically through multiple cell divisions. Similar to other cases of prion

switch, CARD exhibits nucleation- and polymerization-dependent prion conversion in yeast. Likewise, a yeast prion domain (NM) can functionally replace CARD and PYRIN in mammalian innate immune and inflammasome signaling. Mutations in MAVS and ASC that disrupt their prion activities in yeast also abrogate their ability to signal in mammalian cells. Furthermore, fibers of recombinant PYRIN can convert ASC into functional polymers capable of activating caspase-1. Remarkably, homologous domains from a conserved NOD-like receptor (NWD2) and classic prion (HET-s) in fungi can functionally reconstitute signaling of NLRP3 and ASC PYRINs in mammalian cells. These results indicate that prion-like polymerization is a conserved signal transduction mechanism in innate immunity and inflammation.

TABLE OF CONTENTS

PRIOR PUBLICATIONS

**Cai X**, Chen J, Xu H, Liu S, Jiang QX, Halfmann R, Chen ZJ. "Prion-like Polymerization Underlies Signal Transduction in Antiviral Immune Defense and Inflammasome Activation." ***Cell***. 156 (6): 1207-1222 (2014).

**Cai X**, Chiu YH, Chen ZJ. "The cGAS-cGAMP-STING Pathway of Cytosolic DNA Sensing and Signaling." ***Molecular Cell.*** 54 (2): 289-296 (2014).

Liu S, Chen J, **Cai X**, Wu J, Wu YT, Sun L, Chen ZJ. "MAVS recruits multiple ubiquitin E3 ligases to activate antiviral signaling cascades." ***eLife*** 2: e00785 (2013).

LIST OF FIGURES

LIST OF TABLES

# CHAPTER I

# INTRODUCTION

## The Innate Immune System

The innate immune system is an ancient mechanism of self-defense that exists in most, if not all living organisms. The most primitive form may be the bacteria immune defense system called CRISPR (clustered, regularly interspaces short palindromic repeats), which protects bacteria from invading bacteriophages and other plasmids (Horvath and Barrangou, 2010). Here, sequences from invading phages are stably integrated into the host genome as repetitive elements, which are then processed into short RNAs (crRNAs) by CRIPR-associated proteins. These short RNAs then serve as guides for the host CRISPR-associated protein complexes to degrade invading plasmids. Similarly, eukaryotic cells have evolved defense mechanism to degrade foreign nucleic acids through a process known as RNA-mediated interference (RNAi). Infection by viruses results in long double stranded RNA (dsRNA), which are cleaved by the endonuclease Dicer to produce short-interfering RNAs (siRNAs) (Tijsterman and Plasterk, 2004). Similar to crRNA, siRNAs are then used to direct sequence specific degradation of mRNA that contains the same sequence. In all cases, the innate immune system is the first line of hose defense again pathogen invasion and serves as a temporary bandage before a more permanent fix (the adaptive immune system) is activated (Medzhitov, 2010). Its significance is underlied by the fact that deficiency in

components of the innate immune system predisposes the organism to highly infectious diseases and a survival disadvantage (von Bernuth et al., 2008).

**Pattern Recognition Receptors**

In mammals, our innate immune system has evolved to use a number of germline encoded proteins called pattern recognition receptors (PRRs) to distinguish "self" from "non-self" signals (Takeuchi and Akira, 2010). The PRRs detect a class of conserved pathogen motifs that are usually not present on host molecules in order to alert the host that a pathogenic invasion has taken place and to trigger an appropriate host defense in the form of an immune response. For example, Toll-like receptor 4 (TLR4) detects lipopolysaccharide (LPS) from gram-negative bacteria cell-wall and RIG-I detects viral RNAs bearing 5'-triphosphates. The binding of ligands to the PRRs will activate the receptors, which will then initiate several downstream signaling cascades to induce the production of protective cytokines. Innate immune signaling is also essential to activate the adaptive immune system, which uses specific antibodies and lymphocytes tailored against the pathogens. Unlike the delayed and specific nature of adaptive immunity, the innate immune system provides a rapid and generic response to temporarily protect the host through secreted cytokines and other molecules (Medzhitov et al., 2011).

Pattern recognition receptors can be largely grouped into two categories: those that reside on the cell surface plasma memberane and those that reside within the cells in the cytoplasm. For instance, while the Toll-like receptors survey the endosomes and extracellular milieu, cyclic GMP-AMP synthase (cGAS) and retinoic acid-induced gene-I (RIG-I)-like

RNA receptors (RLRs) detect cytosolic DNA and aberrant RNA, respectively, to trigger a robust innate immune response (Sun et al., 2013; Wu et al., 2013; Yoneyama et al., 2004). Table 1 lists some of the most commonly studied PRRs, their ligands, and cellular localization.

| PRRs | Localization | Ligand | Origin |
|---|---|---|---|
| *Toll-like Receptors (TLRs)* | | | |
| TLR1 | Plasma membrane | Triacyl lipoprotein | Bacteria |
| TLR2 | Plasma membrane | Lipoprotein | Bacteria, virus, self |
| TLR3 | Endosomes | dsRNA | Virus |
| TLR4 | Plasma membrane | LPS | Bacteria, virus |
| TLR5 | Plasma membrane | Flagellin | Bacteria |
| TLR6 | Plasma membrane | Diacyl lipoprotein | Bacteria |
| TLR7/8 | Endosomes | ssRNA | Bacteria, virus, self |
| TLR9 | Endosomes | CpG-DNA | Virus, bacteria, self |
| TLR10 | Endosomes | Unknown | Unknown |
| TLR11 | Plasma membrane | Profillin | Protozoa |
| TLR13 | Endosomes | 23S rRNA | Bacteria |
| *RIG-I-like Receptors (RLRs)* | | | |
| RIG-I | Cytoplasm | 5'ppp-RNA | RNA viruses |
| MDA5 | Cytoplasm | Long dsRNA | RNA viruses |
| LGP2 | Cytoplasm | Unknown | RNA viruses |
| *Other Receptors* | | | |
| cGAS | Cytoplasm | DNA | Bacteria, virus, self |
| AIM2 | Cytoplasm | DNA | Bacteria, virus, self |
| NLRP3 | Cytoplasm | Unknown | Unknown |
| NLRC4 | Cytoplasm | Flagellin, T3SS | Bacteria |

**Table 1.** List of pattern recognition receptors, their localization, and their ligands.

**Innate Immune Antiviral Defense**

Viruses are highly infectious pathogens that require host cells to replicate and propagate. Studies on the mechanism of viral replication and antiviral defense have

contributed greatly to our understanding of biology, from the discovery of reverse transcriptase to the realization that functional prion conversion governs important cellular signaling processes (Baltimore, 1995; Moresco et al., 2011). In another instance, studies on innate immune sensing of DNA revealed the first metazoan cyclic dinucleotide, a cyclic GMP-AMP which contains two unique phosphodiester bonds: one between the 2'OH of GMP and the 5'phosphate of AMP and the other between 3'OH of AMP and 5'phosphoate of GMP, hereafter referred to as 2'3'-cGAMP (Gao et al., 2013; Zhang et al., 2013). Viruses can be divided into two large families depending on their nucleic acid content: DNA and RNA viruses. DNA viruses replicate in the nucleus with the exception of poxvirus. On the other hand, RNA viruses, with the exception of influence viruses and retroviruses, mainly replicate in the cytoplasm. Hence, the presence of PRRs in the cytoplasm is essential for the detection of RNA viruses.

The family of RIG-I like receptors (RLR) is the main PRR class that detects cytosolic RNA viruses. RLR contains three members, including RIG-I (Retinoic acid-inducible gene I), MDA5 (melanoma differentiation-associate gene 5), and LGP2 (laboratory of genetics and physiology 2) (Belgnaoui et al., 2011). RIG-I and MDA5 both contain N-terminal CARD (caspase activation and recruitment domains), a middle RNA helicase domain. RIG-I in addition contains a C-terminal regulatory domain. While RIG-I and MDA5 function cooperatively to detect cytosolic viral RNAs, the role of LGP2 in this process is still unclear.

RIG-I usually exist in an autoinhibited state and binds to 5'-triphosphorylated RNA, which are generated following RNA virus infection. Binding to 5'-ppp RNA releases RIG-I from its autoinhibition and frees its N-terminal CARDs [RIG-I(N)] for binding to free lysine 63 (K63)-linked polyubiquitin chains. The binding to polyubiquitin oligomerizes RIG-I into a signaling competent state, allowing it to activate downstream adaptor protein MAVS (mitochondrial antiviral signaling). As a mitochondrial tail anchored protein, MAVS also contains an N-terminal CARD ($MAVS^{CARD}$), which is essential for MAVS activation through CARD-CARD interactions with RIG-I(N). In addition to a CARD, MAVS also contains a middle proline-rich region that contains binding motifs for a number of downstream signaling proteins, and a C-terminal transmembrane domain that targets the protein to the mitochondria. Following activation by RIG-I, MAVS then signals downstream to recruit a number of ubiquitin E3 ligases including TRAF2, 5, and 6, which together synthetize K63-linked polyubiquitins to activate two kinases, IKK and TBK1. The two kinases subsequently activate two transcription factors NF-κB and IRF3, respectively, to induce antiviral cytokine expression including type-I interferons aim to block viral replication and spread (Figure 1).

**MAVS is a functional prion**

Recent mechanistic studies on MAVS activation have indicated that the protein forms functional prion-like polymers to propagate innate immune signaling after activation by RIG-I (Cai et al., 2014; Hou et al., 2011; Zeng et al., 2010). Specifically, after viral infection,

endogenous MAVS forms detergent-resistant, high molecular weight polymers capable of activating the downstream transcription factors NF-κB and IRF3. Under the electron microscope, recombinant MAVS forms fibers that are similar in appears to fibers formed by a fragment of the mammalian prion protein (PrP). Remarkably, active MAVS fibers can catalyze similar biochemical and structural changes to inactivate MAVS, converting them into the active, SDS-resistant polymeric form capable of downstream signaling. These newly converted MAVS polymers resemble those caused by viral infection and gain the ability to activate the transcription factor IRF3.

MAVS contains an N-terminal CARD domain which is responsible for its prion-like behavior and hence is designated as its prion domain. Mutations in CARD that abolish MAVS polymerization also prevent virus-induced, RIG-I-dependent IRF3 activation (Liu et al., 2013), indicating that MAVS polymerization is essential for its function. Interestingly, CARD belongs to the death domain (DD) superfamily that also includes the DD, DED, and PYRIN subfamilies (Park et al., 2007a). Like CARD, members of the DD superfamily regulate cellular signaling through homotypic interactions and the formation of oligomeric complexes.

**ASC-dependent Inflammasome**

The inflammasome is another notable DD containing signaling complex, which is activated as a result of cellular infection or damage and is implicated in numerous diseases (Martinon et al., 2002; Schroder and Tschopp, 2010). ASC is an adapter protein for inflammasome signaling. It is composed of a PYRIN domain ($ASC^{PYD}$) at the N-terminus

and a CARD ($ASC^{CARD}$) at the C-terminus. $ASC^{PYD}$ interacts with PYRINs of activated upstream proteins such as NLRP3 and AIM2, while $ASC^{CARD}$ then relays the signal downstream by binding to the CARD of pro-caspase-1, leading to caspase-1 activation. Activated caspase-1 then cleaves itself and pro-IL-1β, forming p10 and p17 products, respectively, which are then secreted by cells. In response to stimulation, ASC forms high molecular weight oligomers that can be visualized as perinuclear clusters by microscopy (Broz et al., 2010). However, the molecular composition of the inflammasome and the mechanism of ASC activation remain unclear (Broz et al., 2010; Fernandes-Alnemri et al., 2007; Martinon et al., 2002). In similar ways, MAVS and ASC both contain N-terminal domains of the DD family and serve as important signaling hubs that relay signals from multiple upstream sensors to downstream effectors, eventually leading to the secretion of protective cytokines (Figure 1).

**Biology of Prions**

The gain-of-function, beneficial prion-like switch of MAVS is unique among proteins capable of prion conversion (Liebman and Chernoff, 2012). Prion proteins can adopt distinct conformations, at least one of which is self-propagating and heritable upon cell division. They are defined by the ability of a conformationally distinct polymerized form of the protein to convert the soluble, native form of the protein into the polymerized form (Prusiner, 1998).

The discovery of the first prion (now known as the mammalian prion protein) explained a group of puzzling neurodegenerative diseases, where a self-replicating conformation of misfolded PrP is responsible (Prusiner, 1982). Since then, many other prion-

like proteins have been identified. In mammals, prion-like proteins are invariably associated with diseases of protein aggregation (Jucker and Walker, 2013; Ramaswami et al., 2013). However, the idea of beneficial prions has been proposed in yeast and other organisms (Halfmann and Lindquist, 2010; Shorter and Lindquist, 2005; True and Lindquist, 2000). While yeast prions are potential adaptive mechanisms of phenotypic diversification during environmental fluctuation, Aplysia CPEB Drosophila Orb2 prions conversion may underlie memory formation (Majumdar et al., 2012a; Si et al., 2003). In each case, the phenotypic trait is inherited through a self-perpetuating protein conformation.

To further understand MAVS prion conversion and to investigate the possibility that other DD-containing proteins also possess prion-like properties, we sought to reconstitute the prion properties of $MAVS^{CARD}$ and other DDs in yeast, a well-established model organism for studying prions (Alberti et al., 2010). Since the discovery of the first yeast prion 20 years ago, approximately two dozen yeast proteins have been found to acquire self-replicating conformations that act as epigenetic elements of inheritance. Of these, the essential translation termination factor, Sup35, is the best characterized (Liebman and Chernoff, 2012). At its N-terminus, Sup35 harbors a low complexity, intrinsically disordered domain (NM) that undergoes prion conversion. At its C-terminus, Sup35 harbors a globular, catalytic domain (Sup35C) that is responsible for the protein's ability to terminate translation. In its prion state, NM forms amyloid like fibers that sequester the Sup35 protein in an insoluble aggregate, resulting in a reduction in translation termination and a corresponding increase in stop codon read-through that is readily visualized phenotypically. The modular nature of the NM and Sup35C domains as well as the availability of phenotypic reporters for Sup35

activity has popularized the Sup35 based yeast prion assay, which has been instrumental to the discovery of new proteins capable of prion conversion by their ability to functionally replace NM (Alberti et al., 2009; Osherovich et al., 2004; Sondheimer and Lindquist, 2000) (Figure 2).

Here, I use genetic and biochemical assays to demonstrate that MAVS and ASC form prions in yeast in response to upstream sensors and that their prion conversion correlates with their immune and inflammatory signaling abilities. Through reconstitution of the NLRP3 and AIM2 inflammasomes with ASC-Sup35C and pro-caspase-1 in yeast, I show that caspase-1 activation occurs only in yeast clones that harbor the prion form of ASC. Furthermore, I show that recombinant $ASC^{PYD}$ forms prion-like fibers capable of converting inactive ASC into an active prion form necessary and sufficient for downstream signaling. Finally, I demonstrate that homologous domains from a conserved NOD-like receptor and a bona fide prion from a filamentous fungus can together functionally replace NLRP3 and ASC PYRINs in mammalian inflammasome signaling, suggesting that prion-like polymerization is an evolutionarily conserved mechanism of signal transduction.

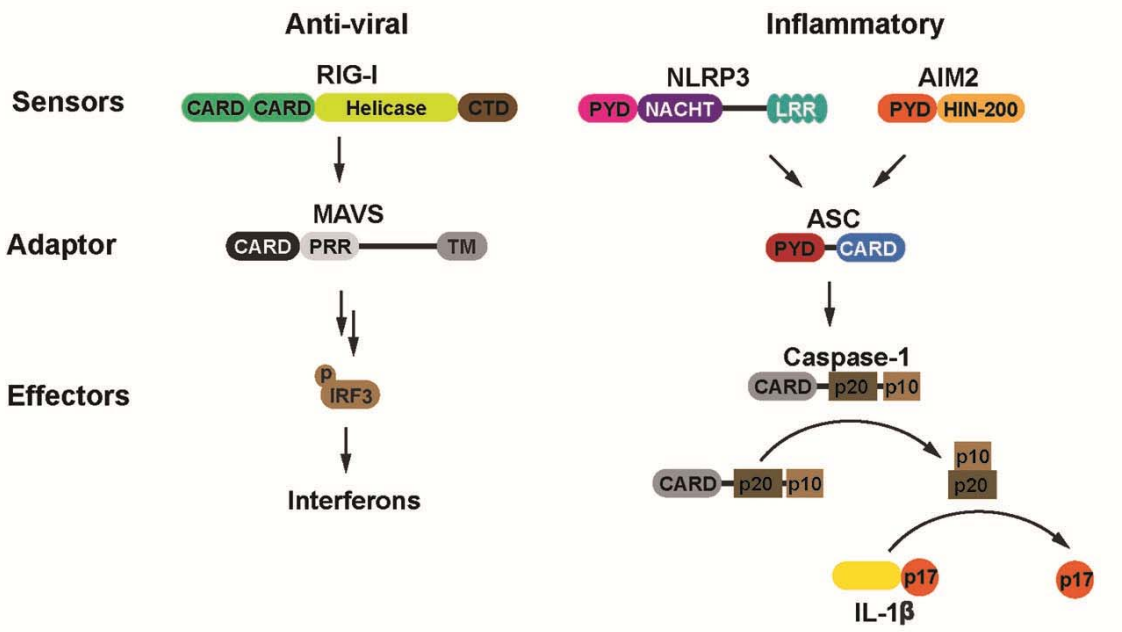


**Figure 1. The RIG-I dependent antiviral pathway and the NLRP3 and AIM2 mediated inflammasome pathway.** Both MAVS and ASC serve as key adaptors to relay multiple upstream signals to downstream effects.

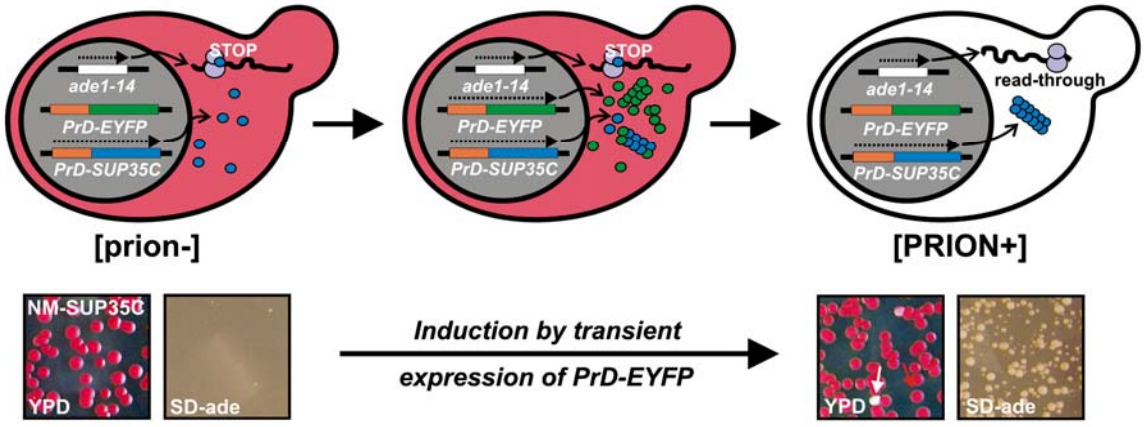


**Figure 2. Cartoon representation of the SUP35 based yeast prion assay.**

In yeast, prion domain (PrD)-SUP35C fusion protein functions as a translation termination factor to prematurely stop the ade1-14 gene, essential for adenine biosynthesis, which contains a nonsense mutation. Cells are red and cannot grown on medium lacking adenine (-ade). When the PrD is overexpresssed, the PrD-Sup35C protein form prions, which compromise its catalytic activity and the protein cannot function as a translation termination factor. The premature stop codon in ade1-14 is read-through leading to functional ade1 production and white colonies that can grow in adenine deficient medium.

# CHAPTER II

# RESULTS

## MAVS$^{CARD}$ is a Functional Prion Domain in Yeast

Hou et. al. recently showed that MAVS$^{CARD}$ forms fibers that can convert endogenous MAVS into high molecular weight, SDS-resistant polymers capable of activating IRF3 (Hou et al., 2011). To determine whether MAVS has other defining properties of prions, we employed the Sup35 based yeast prion assay. We fused MAVS$^{CARD}$ to Sup35C and constitutively expressed the resulting fusion protein in a yeast strain lacking endogenous Sup35 (Figure 2 and 3A). To monitor activity of the fusion protein, the strain also harbored a premature stop codon in *ADE1*, a gene critical for *de novo* adenine biosynthesis. Through the activity of soluble Sup35C, the nonsense *ADE1* mutation blocks the synthesis of functional Ade1, resulting in the accumulation of a red pigment when grown on rich media (YPD or ¼YPD), and an inability to grow on media lacking adenine (-ade). When Sup35 activity is compromised, as when it forms a prion, the stop codon is read through resulting in the synthesis of full length Ade1, a concomitant loss of the red pigment, and growth on -ade media (Chernoff et al., 1995).

The cells expressing MAVS$^{CARD}$-Sup35C formed red colonies on YPD and were unable to grow on -ade media, indicating that the fusion protein was adequately expressed and fully functional. The frequency of prion switching depends on the concentration of the prion protein. Consequently, a defining hallmark of prions is that the prion state can be induced by transient over-expression of the prion protein (Wickner, 1994). To this end, we

transformed the MAVS$^{CARD}$-Sup35C strain with a plasmid driving the expression of MAVS$^{CARD}$-EYFP from the inducible *GAL1* promoter. Following transient expression of MAVS$^{CARD}$-EYFP in galactose-containing media, we plated the cells to glucose-containing, nonselective media, on which MAVS$^{CARD}$-EYFP was no longer expressed. This treatment produced white colonies on ¼YPD, indicating a self-perpetuating state that is stable over numerous cell divisions. Furthermore, we observed red/white sectored colonies suggesting the phenotype is bi-stable and unlikely to be due to genetic mutations (Figure 3B). Similarly, when plated to adenine deficient glucose-containing medium (SD-ade), the transient expression of MAVS$^{CARD}$-EYFP, but not NM-EYFP, produced a high frequency of Ade+ colonies, each derived from a cell that had heritably acquired the ability to synthesize adenine (Figure 3C). From the fivefold serial dilutions on SD-ade, we estimate that transient expression of MAVS$^{CARD}$ increased the frequency of Ade+ colonies by ~125 fold.

We next sought to determine if the Ade+ phenotype of MAVS$^{CARD}$-Sup35C yeast is cytoplasmically inherited, a signature of all prions. To this end, we performed a series of cytoduction experiments, in which the cytoplasm but not the nucleus is transferred from one yeast strain (donor) to another (recipient), which contains a *kar1* mutation that blocks nuclear fusion. Haploid daughter cells (cytoductants) are subsequently recovered that have specifically lost the donor nucleus but now contain cytoplasm from both parents (Figure 4). When an Ade+ donor was cytoduced with an ade- recipient (both expressing MAVS$^{CARD}$-Sup35C), over 40% of the cytoductants were Ade+, indicating that the Ade+ phenotype is inherited cytoplasmically without nuclear contribution (Figure 4). The ade- cytoductants in this case result from a subpopulation of ade- cells in the Ade+ parent cell population (as

evidenced by red sectors in the Ade+ donor spot), due to spontaneous loss of the prion state. Cytoduction between two ade- strains uniformly produced ade- cytoductants.

To assess whether the Ade+ phenotype is dominant and dependent on the $MAVS^{CARD}$-Sup35C fusion protein, we performed a series of plasmid shuffle experiments as outlined in Figure 5. First, we mated haploid Ade+ cells of mating type a (MATa) with haploid ade- cells of MATα. The two strains each expressed $MAVS^{CARD}$-Sup35C from differentially marked plasmids (Leu+ or Trp+). We then assayed Sup35C function in diploids that had lost the original $MAVS^{CARD}$-Sup35C construct of the Ade+ MATa parent. The resultant leu-, Trp+ diploids retained a pink color and the ability to grow on SD-ade, indicating that the Ade+ phenotype is dominant (Figure 5). As a control, mating between two ade- strains resulted in red cells that did not grow on SD-ade (Figure 5). However, when either Ade+ or ade- $MAVS^{CARD}$-Sup35C yeast was mated with an ade- haploid expressing an unrelated DD-Sup35C fusion ($ASC^{PYD}$-Sup35C), the resultant diploids that have lost the $MAVS^{CARD}$-Sup35C plasmid were red with similar background growth on SD-ade. These results demonstrate that the Ade+ phenotype requires the continued expression of $MAVS^{CARD}$-Sup35C. We conclude that $MAVS^{CARD}$ is a bona fide prion protein when expressed in yeast. In keeping with standard prion nomenclature, we designate its prion state [$MAVS^{CARD}$+], with capitals and brackets denoting genetic dominance and cytoplasmic inheritance, respectively. The native (prion minus) state of MAVS CARD is denoted as [$mavs^{card}$-]. The [$MAVS^{CARD}$+] phenotype is similar to that of yeast containing the prion form of WT Sup35, [*PSI*+] (data not shown).

Given that $MAVS^{CARD}$ functionally replaces $Sup35^{NM}$ as a yeast prion, we tested the converse: whether substituting $MAVS^{CARD}$ with NM (NM-MAVS, Figure 3A) could activate IRF3 in the mammalian system. We have recently described a cell-free system that recapitulates MAVS polymer dependent IRF3 activation, where incubation of $MAVS^{CARD}$ fibers with mitochondria (containing MAVS), along with cytosolic extracts and $^{35}$S-IRF3 substrate results in IRF3 dimerization, the hallmark of its activation (Figure 6A). Incubation of recombinant NM fibers with mitochondria from HEK293T cells stably expressing NM-MAVS resulted in robust IRF3 dimerization, whereas incubation of NM with control mitochondria (containing endogenous MAVS) did not (Figure 6B). Incubation of mitochondria containing NM-MAVS with fibers formed from a fragment of the mammalian prion protein (PrP) (Hou et al., 2011) also did not activate IRF3 *in vitro*, demonstrating that NM-MAVS activation by prion fibers is sequence specific

Next, we sought to determine if NM-MAVS could signal in cells. NM fibers are capable of entering mammalian cells through an unknown mechanism (Ren et al., 2009). Using a 293T cell line that contains a luciferase gene driven by the interferon-β promoter (*IFN β* -Luc 293), we added NM fibers to the culture media of cells transfected with either NM alone or NM-MAVS. Luciferase activity assay showed that NM fibers markedly enhanced IFNβ induction in cells expressing NM-MAVS but not in those expressing NM (Figure 6C). Consistent with our *in vitro* assay, these data indicate that NM fibers induce a specific conformational switch in NM-MAVS that is sufficient for downstream IRF3 activation, functionally similar to the prion switch induced in endogenous MAVS by $MAVS^{CARD}$.

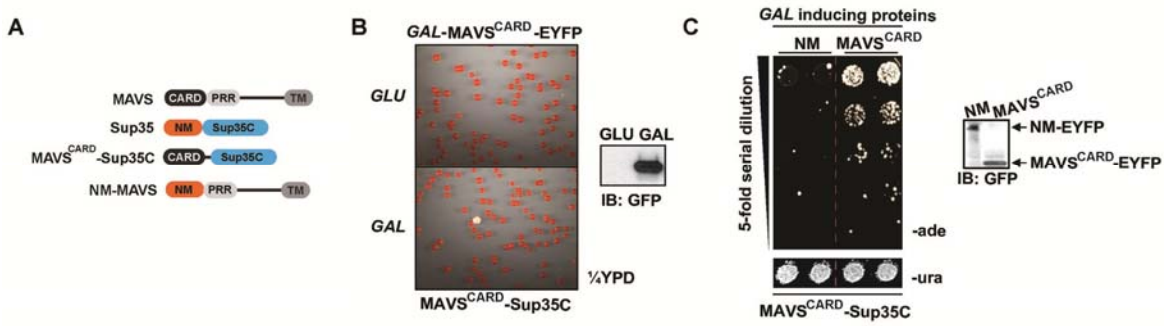


**Figure 3. MAVS$^{CARD}$ is a functional prion in yeast.**

(A) Cartoon depictions of MAVS, Sup35, MAVS$^{CARD}$-Sup35C and NM-MAVS proteins.
(B) Cells from a single yeast colony harboring constitutively expressed MAVS$^{CARD}$-Sup35C and galactose inducible (*GAL*-)MAVS$^{CARD}$-EYFP (Ura+) were grown for 48 hours in media containing either galactose (SG-ura) or glucose (SD-ura), followed by plating onto ¼YPD at a density of ~500 cells/plate. Induction of MAVS$^{CARD}$-EYFP was monitored by western blotting with a GFP antibody.
(C) Single yeast colonies harboring constitutively expressed MAVS$^{CARD}$-Sup35C and *GAL*-NM-EYFP or *GAL*-MAVS$^{CARD}$-EYFP (Ura+) were grown in SD-ura for 24 hours to equal density followed by growth in SG-ura for 48 hours. Two colonies of each were plated onto non prion-selective media (SD-ura) and prion-selective, adenine-deficient media (SD-ade) at five-fold serial dilutions. One dilution on SD-ura is shown as an indicator of equal plating density among the samples. Expression of NM- and MAVS$^{CARD}$-EYFP was monitored by western blotting with a GFP antibody. Dotted red line in this and other figures indicates serial dilutions grown non-adjacently on the same plate.

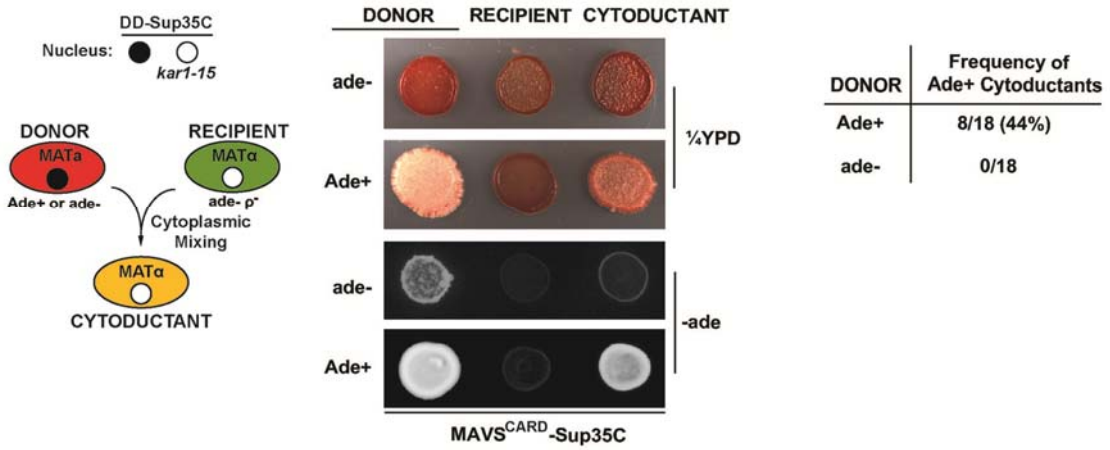


**Figure 4. MAVS$^{CARD}$ prion state is cytoplasmically inherited.**

Left: A schematic for the cytoduction experiments. Ade+ or ade- donor strain harboring death domain (DD)-Sup35C fusion (e.g., MAVS$^{CARD}$-Sup35C) was cytoduced into a recipient strain expressing the same DD-Sup35C fusion and a *kar1* mutation (*kar1-15*) which prevents nuclear fusion. Haploid cytoductants, containing both parental cytoplasms but only the recipient nucleus, were selected. Middle: Representative single clones of Ade+ or ade- donors, ade- recipients, or resultant cytoductants each expressing MAVS$^{CARD}$-Sup35C were plated onto ¼YPD and SD-ade. Right: A table showing the frequency of Ade+ cytoductants from Ade+ or ade- donors harboring MAVS$^{CARD}$-Sup35C.

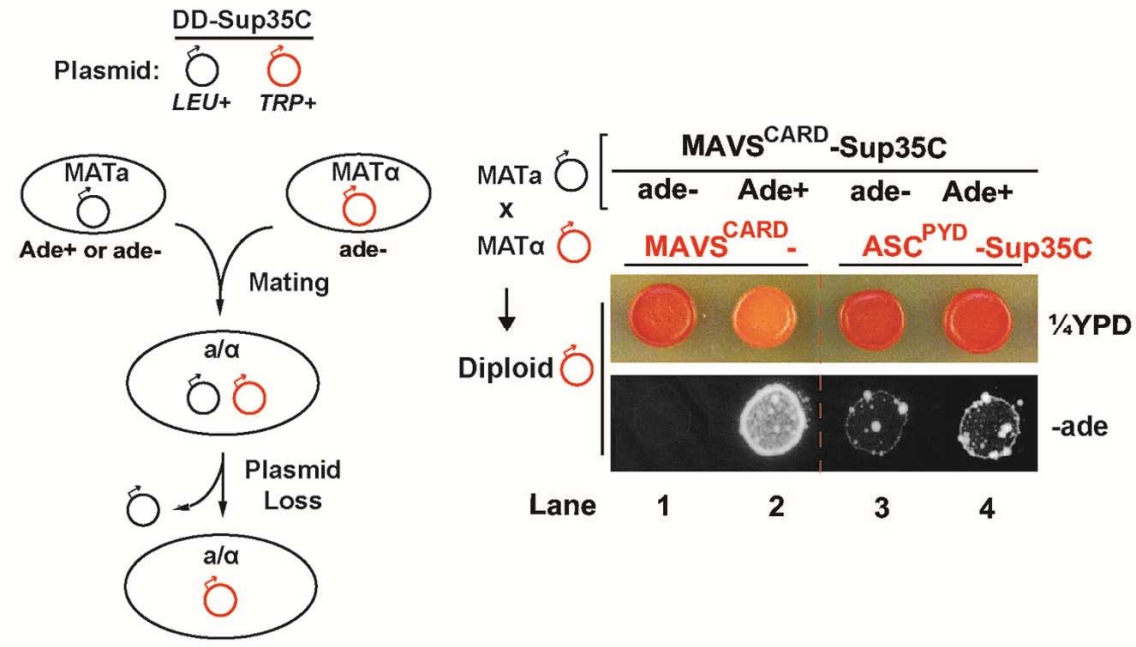


**Figure 5. MAVS$^{CARD}$ prion state is dominant.**

Left: A schematic for the mating and plasmid shuffle experiments. Ade+ or ade- haploid yeast of mating type a (MATa) expressing DD-Sup35C fusion from a Leu+ plasmid (black circle) were mated with an ade- MATα strain harboring DD-Sup35C on a Trp+ plasmid (grey circle), followed by selection for diploids that have lost the original DD-Sup35C Leu+ plasmid. The resultant DD-Sup35C leu- Trp+ cells were assessed for the prion phenotype. Right: An ade- or Ade+ MATa strain of MAVS$^{CARD}$-Sup35C was mated with an ade- MATα strain harboring either MAVS$^{CARD}$-Sup35C or ASC$^{PYD}$-Sup35C following the protocol outlined above. Representative single colonies of diploid leu- Trp+ cells were plated onto ¼YPD and SD-ade.

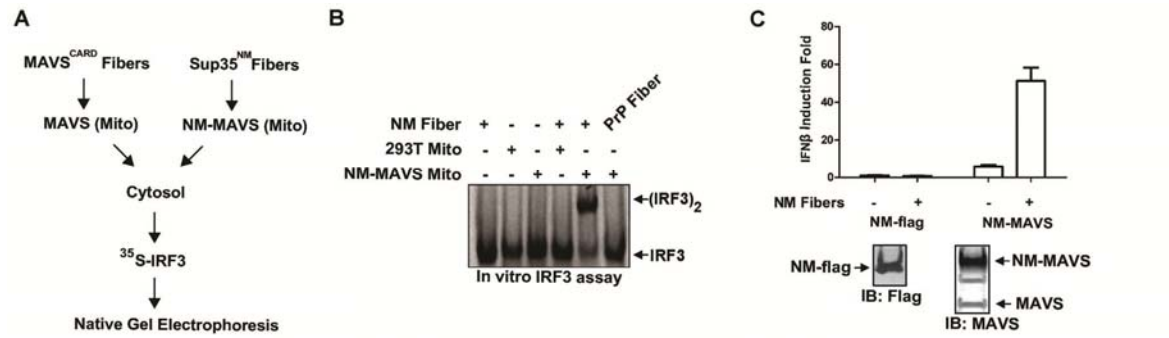


**Figure 6. SUP35$^{NM}$ replaces MAVS$^{CARD}$ in mammalian cells.**

(A) Schematic representation of an IRF3 *in vitro* assay that recapitulates MAVS$^{CARD}$ and NM prion activity and signaling *in vitro*.
(B) Mitochondrial fractions from parental 293T or those expressing NM-MAVS were incubated with NM or PrP fibers as indicated at RT for 30 minutes, followed by incubation with 293T cytosolic extract, MgATP buffer, and $^{35}$S-IRF3 at 30°C for 60 minutes. Dimerization of IRF3, indicative of its activation, was visualized by autoradiography following native gel electrophoresis.
(C) NM-flag or NM-MAVS was transfected into 293T-*IFNβ*-luciferase reporter cells. Recombinant NM fibers were added to the culture media twenty-four hours later and allowed to incubate for additional 24 hours, followed by luciferase reporter assay. Expression of NM-flag was monitored by a Flag antibody and NM-MAVS by a MAVS antibody. Error bar represents standard deviation of triplicates.

**RIG-I(N) Converts MAVS$^{CARD}$ into Prion in Yeast**

In mammalian cells, over-expression of the N-terminal tandem CARDs of RIG-I [RIG-I(N)] is sufficient to activate MAVS (Seth et al., 2005). To determine if RIG-I could trigger the prion-like conversion of MAVS in the yeast prion assay, we transiently expressed RIG-I(N) in the MAVS$^{CARD}$-Sup35C strain, followed by plating the cells onto ¼YPD or onto SD-ade. Expression of RIG-I(N) resulted in a high frequency of white colonies on ¼YPD and a ~3000 fold increase in the frequency of Ade+ colonies as compared to expression of NM (Figures 7A and 7B). The much higher frequency of prion conversion induced by RIG-I(N) as compared to MAVS$^{CARD}$ suggests that the physiological upstream sensor is more potent at nucleating MAVS$^{CARD}$ polymerization. Instead of forming self-perpetuating fibers, RIG-I(N) has recently been shown to form a tetramer in the presence of K63 polyubiquitin chains (Jiang et al., 2012). In contrast to the observed prion conversion of MAVS$^{CARD}$, transient expression of RIG-I(N) was unable to induce Ade+ colonies in cells harboring RIG-I(N)-Sup35C, consistent with RIG-I's role as an upstream prion-nucleating factor rather than a prion itself (Figure 8). Recently, we identified a number of conserved MAVS$^{CARD}$ residues that, when mutated to alanine, abolished virus-induced IRF3 activation (Liu et al., 2013). Consistent with their inability to signal in the mammalian system, E26A, R64A, and R65A MAVS$^{CARD}$-Sup35C were defective in RIG-I(N)-induced prion formation (Figures 9). Surprisingly, however, when we incubated 293T lysate expressing WT or mutant flag-MAVS$^{CARD}$ with mitochondria from parental 293T cells, only R65A and R64A/R65A MAVS$^{CARD}$ were defective in inducing endogenous MAVS to activate IRF3 *in vitro* (Figure 10A).

Unlike amorphous protein aggregation, prions polymerize in an ordered process that proceeds through a rate limiting nucleation step followed by rapid, energetically favorable polymerization (Collins et al., 2004; Serio et al., 2000). The Sup35 based yeast prion assay can uncouple the effects of prion nucleation and polymerization, allowing us to probe the mechanistic differences between MAVS$^{CARD}$ mutants. Specifically, defects in nucleation can be revealed during de novo prion formation, mediated by transient expression of the inducing protein. Defects in polymerization, in contrast, can be revealed by the efficiency with which the protein perpetuates pre-existing prions, which is responsible for the phenotypic readout. Consistent with our *in vitro* assay in Figure 10A, only R65A MAVS$^{CARD}$ failed to induce MAVS$^{CARD}$-Sup35C prion conversion in yeast (Figures 10B),suggesting that R65A is unable to nucleate WT MAVS prion conversion whereas E26A and R64A have no such defect. To test if these mutants instead block polymerization, we supplied prion templates in the form of transiently expressed WT MAVS$^{CARD}$-EYFP in yeast strains expressing WT or mutant MAVS$^{CARD}$-Sup35C. Here, all three mutants of MAVS$^{CARD}$-Sup35C were unable to propagate as prions (Figure 10C), suggesting that each of these mutations abrogates MAVS polymerization. Thus, as for other prions, MAVS$^{CARD}$ prion formation is a multi-step process comprised of separable nucleation and polymerization steps. Importantly, our finding that E26A and R64A mutants of MAVS are defective in polymerization but not nucleation, together with our previous results that these mutants are defective in supporting IRF3 activation and IFN induction by RNA viruses (Liu et al., 2013), indicate that the MAVS nucleation alone is insufficient to activate the downstream signaling cascades. Rather, both nucleation and polymerization are required for MAVS activation. Together with our previous

report, these results firmly establish MAVS as a bona fide prion and validate the Sup35 based yeast prion assay as an attractive means for identifying and characterizing other prions.

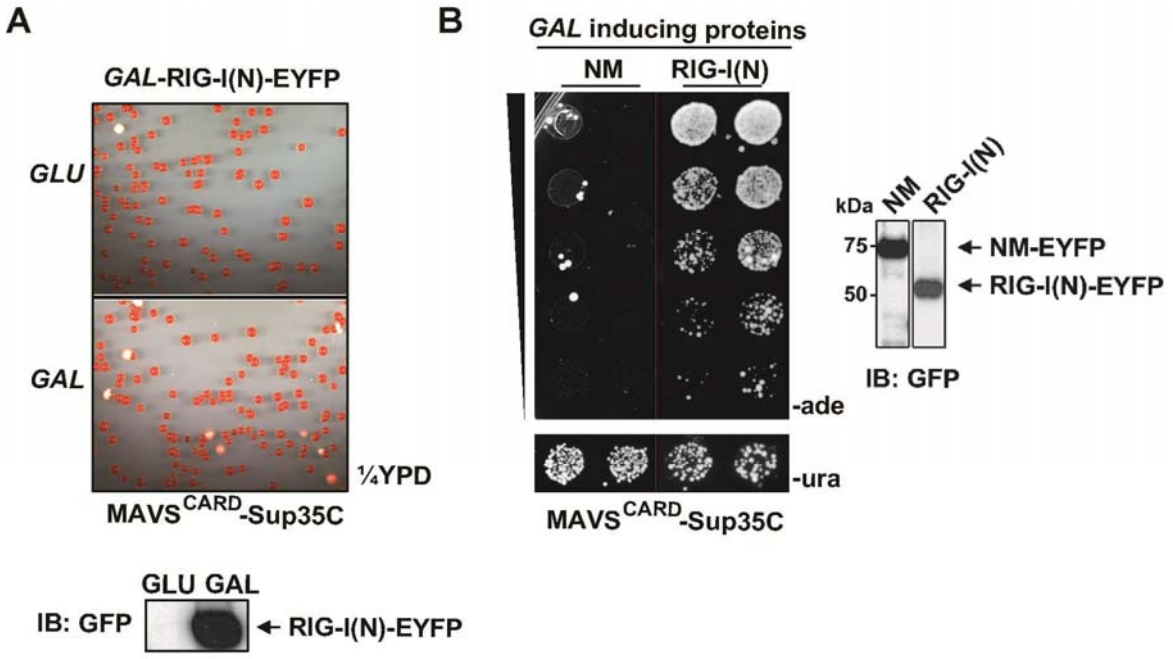


**Figure 7. RIG-I(N) nucleates MAVS$^{CARD}$ prion conversion in yeast.**

(A) A single yeast colony harboring constitutively expressed MAVS$^{CARD}$-Sup35C and *GAL*-RIG-I(N)-EYFP (Ura+) was grown in SD-ura (top) or SG-ura (bottom) for 48 hours followed by plating onto ¼YPD at a density of 500 cells/plate. Expression of RIG-I(N)-EYFP was monitored by Western blotting with a GFP antibody.
(B) Single yeast colonies harboring MAVS$^{CARD}$-Sup35C and NM- or RIG-I(N)-EYFP were grown in SD-ura to equal density followed by growth in SG-ura for 48 hours before plating of five-fold serial dilutions onto SD-ade and SD-ura. Two independent colonies of each are shown. One row of serial dilutions on SD-ura is shown. Expression of NM and RIG-I(N) were monitored by Western blotting with a GFP antibody. The solid red line in this and other figures indicates serial dilutions grown under the same conditions on separate plates in the same experiment.

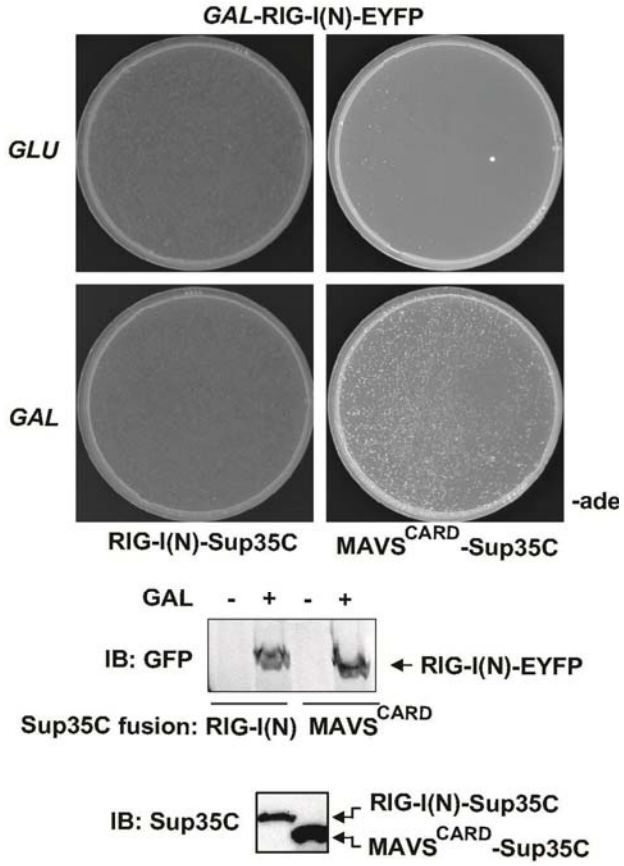


**Figure 8. RIG-I(N) is not a prion.**

SUP35 assay using RIG-I(N)-SUP35C fusion reveals that RIG-I(N) is not a prion in yeast.

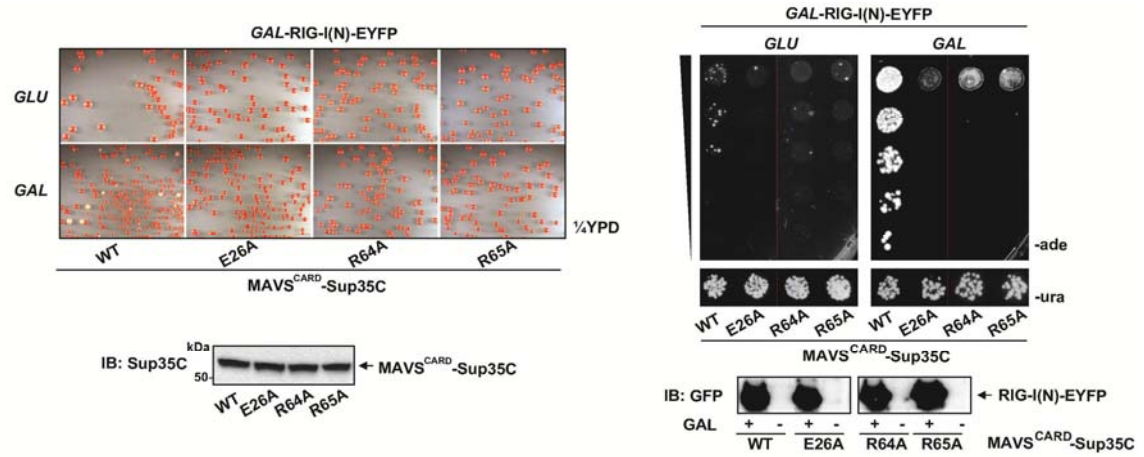


**Figure 9. RIG-I(N) nucleates MAVS$^{CARD}$ prion conversion in yeast.**

(A) Single yeast colonies harboring constitutively expressed WT or mutant MAVS$^{CARD}$-Sup35C and *GAL*-RIG-I(N)-EYFP were grown for two days in SD-ura or SG-ura followed by plating of five-fold serial dilutions onto SD-ade and SD-ura. One row of SD-ura was shown to indicate similar plating cell densities among the samples. Galactose induced expression of RIG-I(N)-EYFP was monitored by Western blotting with a GFP antibody (bottom).
(B) Similar to (A), except that cells were plated onto ¼YPD at a density of 500 cells/plate.

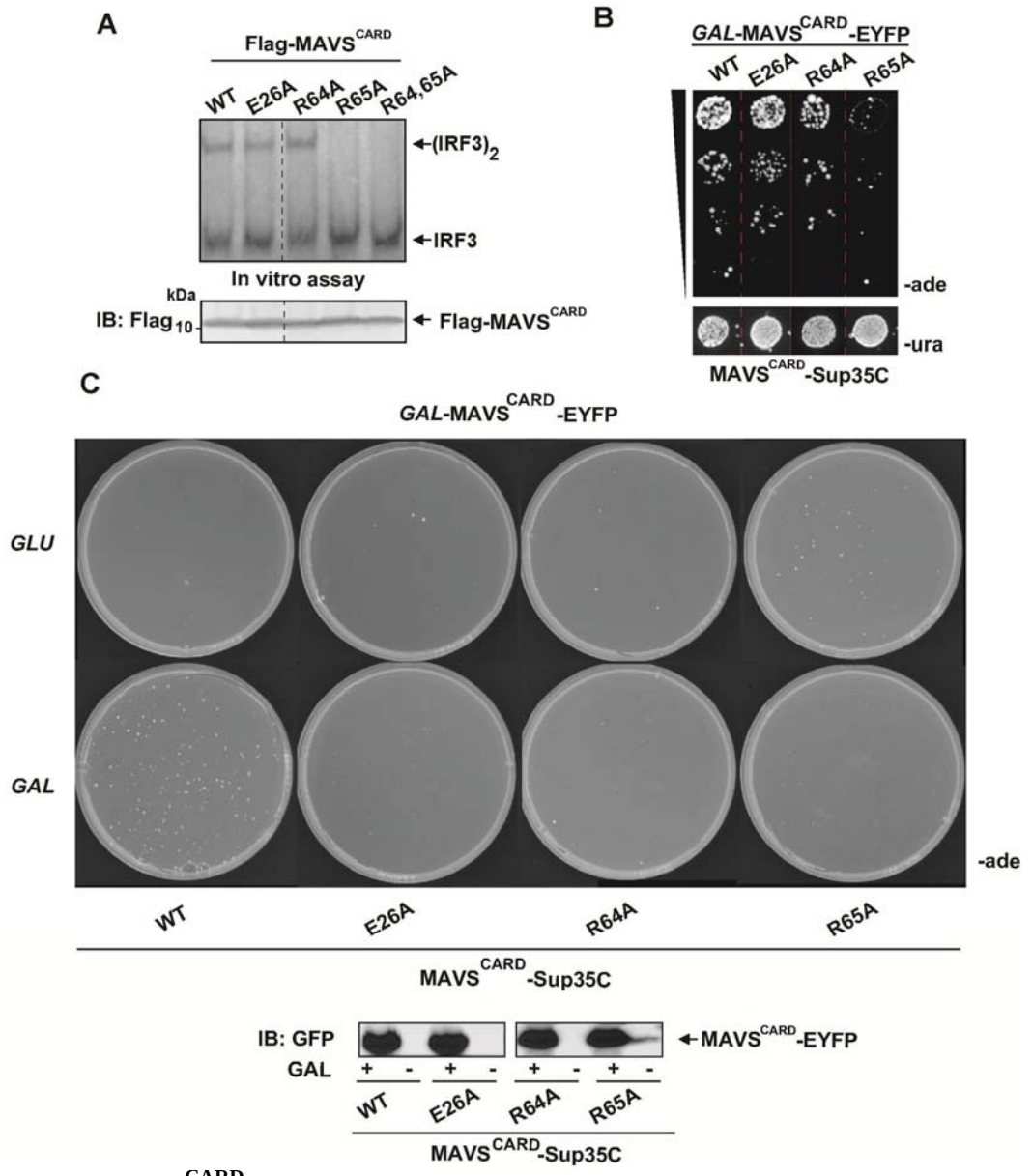


**Figure 10. MAVS$^{CARD}$ exhibits two stage prion conversion.**

(A) Mitochondrial fractions from parental 293T cells were incubated at RT for 10 minutes with cell lysates of 293T cells expressing WT or mutant MAVS$^{CARD}$, followed by incubation at 30°C for 60 minutes with parental 293T cytosolic extracts, MgATP buffer, and $^{35}$S-IRF3. Dimerization of IRF3 was visualized by autoradiography following native gel electrophoresis. Expression of MAVS$^{CARD}$ was monitored by Western blotting with a Flag antibody.
(B) Single yeast colonies harboring constitutively expressed WT MAVS$^{CARD}$-Sup35C and WT or mutant *GAL*-MAVS$^{CARD}$-EYFP were grown to equal density in SD-ura followed by growth in SG-ura for two days, followed by plating of five-fold serial dilutions onto SD-ade and SD-ura. One row of the SD-ura plate is shown. Expression of MAVS$^{CARD}$-EYFP was monitored by Western blotting using a GFP antibody (bottom).
(C) Single yeast colonies harboring constitutively expressed WT or mutant MAVS$^{CARD}$-Sup35C and WT *GAL*-MAVS$^{CARD}$-EYFP were grown in SD-ura or SG-ura for two days before plating onto SD-ade at a density of 50,000 cells per plate. Expression of MAVS$^{CARD}$-EYFP and MAVS$^{CARD}$-SUP35C was monitored using a GFP and Sup35C antibody, respectively.

**Characterization of ASC$^{PYD}$ as a Prion Domain**

To identify other DD superfamily members that may behave as prions, we used the Sup35 system to screen eighteen additional DDs, spanning all four subfamilies (Figure 11A). Several of the DD-Sup35C strains exhibited uniform white colors on YPD, indicating a high basal level of stop codon read-through due either to insufficient expression or to low basal activity of the fusion protein. Of the remaining strains, the one expressing ASC$^{PYD}$-Sup35C formed predominantly dark red colonies with an appreciable frequency of white colonies (Figure 11B), suggesting that ASC$^{PYD}$-Sup35C sufficiently rescues WT Sup35 function and also exhibits a strong tendency for prion formation.

To explore the putative prion properties of ASC, we transiently expressed ASC$^{PYD}$-EYFP in a red ASC$^{PYD}$-Sup35C isolate. Remarkably, this increased the appearance of Ade+ colonies and the appearance of both white and white/red sectored colonies on ¼YPD, suggesting that ASC$^{PYD}$ behaves as a functional prion domain in yeast (Figure 12A). To determine if ASC prion conversion can be induced by upstream sensors, we investigated the prion conversion of ASC$^{PYD}$-Sup35C upon transient expression of NLRP3$^{PYD}$ and AIM2$^{FL}$ in yeast. Over-expression of NLRP3$^{PYD}$ or AIM2$^{FL}$ has been shown to activate the inflammasome in mammalian cells (Hornung et al., 2009). As shown in Figure 12B and 12C, transient expression of NLRP3$^{PYD}$ and AIM2$^{FL}$ increased the frequency of white and Ade+ colonies. Interestingly, the effect from these proteins was much stronger than had been observed for ASC$^{PYD}$ induction. Moreover, AIM2 was unable to induce prion formation in ASC$^{CARD}$-Sup35C harboring strains, consistent with the model that the PYRIN domains of upstream sensors activate ASC through PYRIN-PYRIN interactions (Figure 12D). Next, we

examined the specificity of ASC$^{PYD}$ prion conversion by upstream signaling proteins. IFI16 and IFI204 also harbor N-terminal PYRINs; however, they were unable to induce prion switching by ASC$^{PYD}$ (Figure 13A). Moreover, a strain harboring NLRP3$^{PYD}$-Sup35C was unable to undergo prion conversion following ASC$^{PYD}$, NLRP3$^{PYD}$, or AIM2$^{FL}$ expression, treatments that did induce prion conversion of ASC$^{PYD}$-Sup35C (Figure 13B). Together, these results demonstrate that, just as we had observed for MAVS$^{CARD}$, the physiological upstream signaling proteins of ASC$^{PYD}$ nucleate prion formation more potently than the prion domain itself, but are not prions themselves.

Next, to investigate the mode of inheritance of the Ade+ phenotype, we performed cytoduction experiments as described in Figure 4 with strains harboring ASC$^{PYD}$-Sup35C. Ade+ but not ade- donor strains produced haploid cytoductants that were Ade+ and white on ¼YPD, indicating that the Ade+ phenotype of ASC$^{PYD}$-Sup35C is cytoplasmically inherited (Figure 12E). Furthermore, mating between Ade+ and ade- yeast followed by a plasmid shuffle as described in Figure 1E resulted in uniformly Ade+ diploids, and the Ade+ phenotype required the continued presence of the ASC$^{PYD}$-Sup35C plasmid (Figure 12F, lanes 2 and 4). No Ade+ yeast were observed after crossing two ade- strains (lane 1). These results indicate that the Ade+ phenotype of ASC$^{PYD}$-Sup35C is dominant, requires the continued expression of ASC$^{PYD}$-Sup35C, and cannot be transmitted to MAVS$^{CARD}$. Taken together, we conclude that ASC$^{PYD}$ acquires a prion state in yeast, which we hereafter designate [*ASC*$^{PYD}$+]. To confirm that ASC$^{PYD}$ had undergone a conformational switch in the [*ASC*$^{PYD}$+] cells, we performed semi-denaturing detergent-agarose gel electrophoresis (SDD-AGE), a technique commonly used to detect SDS-resistant polymers of prion proteins

(Halfmann and Lindquist, 2008). We have previously employed the SDD-AGE assay to show that activated MAVS forms high molecular weight polymers (Hou et al., 2011). Similarly, the same analysis revealed that [*ASC*$^{PYD}$+], but not [*asc*$^{pyd}$-] cells, harbor SDS-resistant polymers of ASC$^{PYD}$-Sup35C, as detected with a Sup35C antibody (Figure 12G).

Next, we tested whether the NM prion domain from Sup35 could functionally replace ASC$^{PYD}$ in activating downstream caspase-1. Together with lysate from 293T cells stably expressing pro-caspase-1 (293T+pro-caspase-1) as the substrate, incubation of recombinant NM fibers with lysate from 293T cells expressing NM-ASC$^{CARD}$, but not NM-ASC$^{PYD}$ fusion, resulted in caspase-1 activation *in vitro* (Figure 12H). Moreover, the addition of NM fibers to 293T cells stably expressing pro-caspase-1, pro-IL-1β, and NM-ASC$^{CARD}$ resulted in the secretion of active IL-1β, p17 (Figure 12I). In contrast, the cells expressing NM-ASC$^{PYD}$ did not activate the inflammasome. Hence, a yeast prion domain can functionally replace ASC$^{PYD}$ in inflammasome signaling. From these results, we conclude that ASC undergoes a prion-like switch to activate downstream signaling.

A

| No. | Domain | Color on ¼YPD | *Spontaneous White Colony |
|---|---|---|---|
| 1 | APAF1 CARD | Red | No |
| 2 | ASC CARD | Red | No |
| 3 | ASC PYD | Red | **Yes** |
| 4 | BCL10 CARD | White | #N/A |
| 5 | CARMA1 CARD | Red | No |
| 6 | CASP8 DEDs | N/A | N/A |
| 7 | CASP9 CARD | Pink | No |
| 8 | FADD DD | Red | No |
| 9 | FADD DED | White | N/A |
| 10 | FAS DD | Red | No |
| 11 | MALT1 DD | White | N/A |
| 12 | MYD88 DD | N/A | N/A |
| 13 | NLRP3 PYD | Red | No |
| 14 | NOD1 CARD | Pink | No |
| 15 | NOD2 CARDs | N/A | N/A |
| 16 | RIP1 DD | Pink | **Yes** |
| 17 | RIP2 CARD | Pink | No |
| 18 | TRADD DD | White | N/A |

N/A: cells did not survive 5-FOA selection (see Experimental Procedures).
*Spontaneous white colony appearance without any stimulation.
# Non-applicable (N/A in last column).

B


**Figure 11. DD candidate screen for other prions.**

(A) A list of eighteen DDs and the colors of their DD-Sup35C fusion yeast strains on YPD. Red, pink, and white colors on YPD indicate normal, low, and very low levels of Sup35C activity, respectively, as compared to WT Sup35. The spontaneous appearance of white colonies was observed as indicated.
(B) A single yeast clone expressing $ASC^{PYD}$-Sup35C on the constitutive TEF2 promoter was streaked to ¼YPD. The spontaneous appearance of a white colony is seen in the foreground.

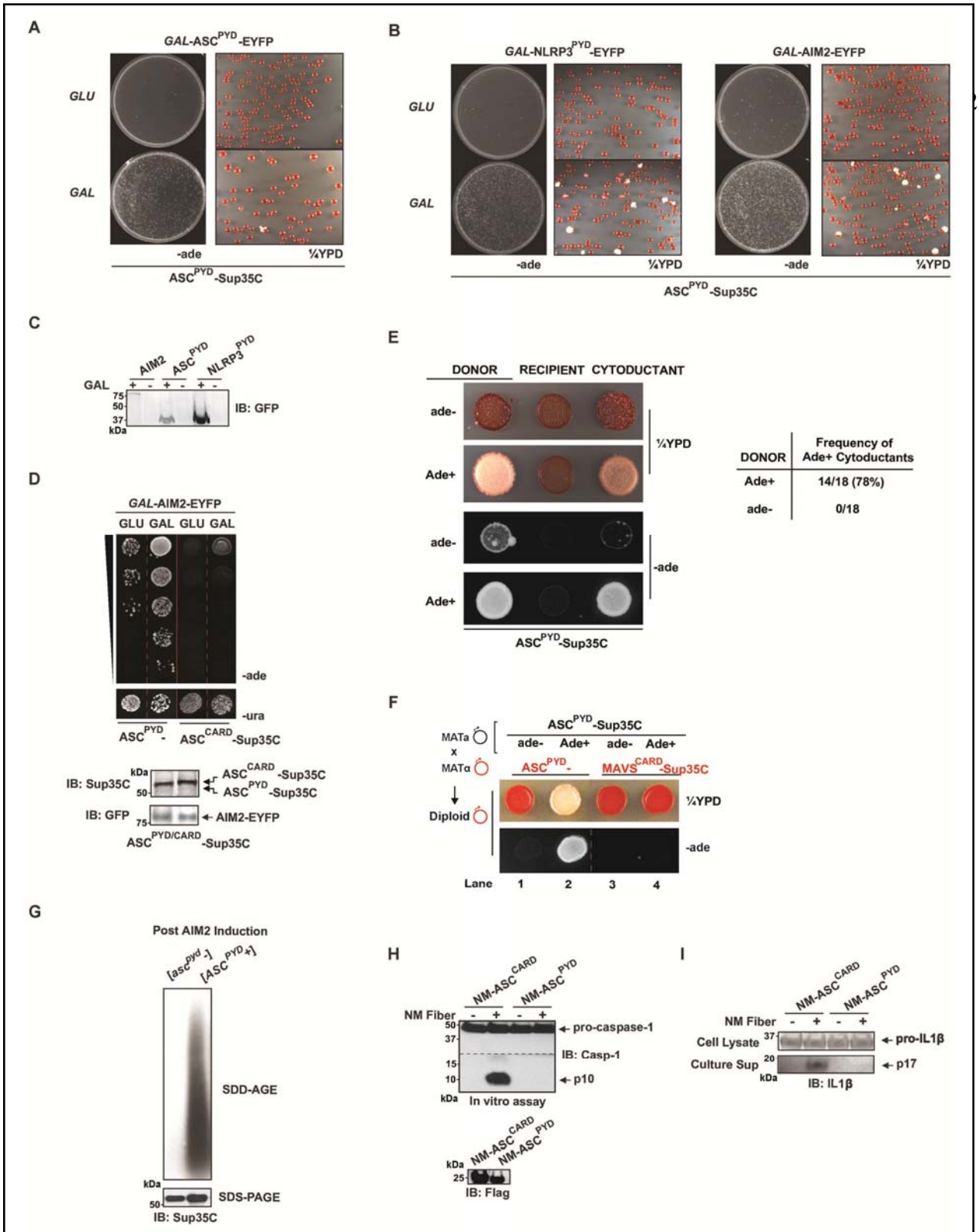


**Figure 12. ASC$^{PYD}$ in a prion in yeast.**

Legends continued on the next page.

**Figure 12 Legends continued.**

(A) A single yeast colony harboring constitutively expressed $ASC^{PYD}$-Sup35C and *GAL*-$ASC^{PYD}$-EYFP (Ura+) was grown in SD-ura or SG-ura for two days followed by plating onto SD-ade and ¼YPD at a density of 100,000 and 500 cells/plate, respectively.
(B) Similar to (A), except that $NLRP3^{PYD}$ or $AIM2^{FL}$, instead of $ASC^{PYD}$, was used to induce $ASC^{PYD}$ prion formation.
(C) GAL inducible protein expression in (A) and (B) is monitored by immunoblotting with a GFP antibody.
(D) Single yeast colonies with constitutively expressed $ASC^{PYD}$-Sup35C or $ASC^{CARD}$-Sup35C and *GAL*-$AIM2^{FL}$-EYFP were grown in SD-ura or SG-ura for two days followed by plating of five-fold serial dilutions onto SD-ade and SD-ura. One serial dilution on SD-ura is shown. Expression of Sup35C fusions and $AIM2^{FL}$ was monitored by a Sup35C and GFP antibody, respectively.
(E) Left: Following cytoduction as depicted in Figure 1D, representative single clones of Ade+ or ade- donors, ade- recipients, and resultant cytoductants each expressing $ASC^{PYD}$-Sup35C were plated onto ¼YPD or SD-ade. Right: A table showing the frequency of Ade+ cytoductants from Ade+ or ade- donors harboring $ASC^{PYD}$-Sup35C.
(F) Mating between an ade- or Ade+ MATa strain with an ade- MATα strain each harboring differentially marked DD-Sup35C was carried out as depicted in Figure 1E. Representative resultant diploid leu- Trp+ single colonies were plated onto ¼YPD or SD-ade. Lanes are numbered as described in the text.
(G) Following induction by $AIM2^{FL}$ expression, colonies with soluble or prion form of $ASC^{PYD}$ ([$asc^{pyd}$-] or [$ASC^{PYD}$+], respectively) were subjected to SDD-AGE analysis for SDS-resistant polymers and SDS-PAGE for expression levels.
(H) NM-$ASC^{PYD}$ or NM- $ASC^{CARD}$ was transiently transfected into 293T cells. Twenty-four hours later, cell lysates were incubated with recombinant NM fibers at RT for 30 minutes, then an aliquot of the lysates was incubated at 30° for 60 minutes with extracts from 293T cells stably expressing pro-caspase-1, followed by western analysis for caspase-1 activation. Expression of NM-$ASC^{PYD}$ or NM- $ASC^{CARD}$ was monitored by immunoblotting to detect the C-terminal flag tag.
(I) NM-$ASC^{PYD}$ or NM- $ASC^{CARD}$ was transiently transfected into 293T cells stably expressing pro-caspase-1 and pro-IL1β. Twenty-four hours later, NM fibers were added to the culture media and allowed to incubate for 24 hours, followed by immunoblotting of the culture supernatant and cell lysates to detect secreted p17 fragment of IL1β and pro-IL1β, respectively.

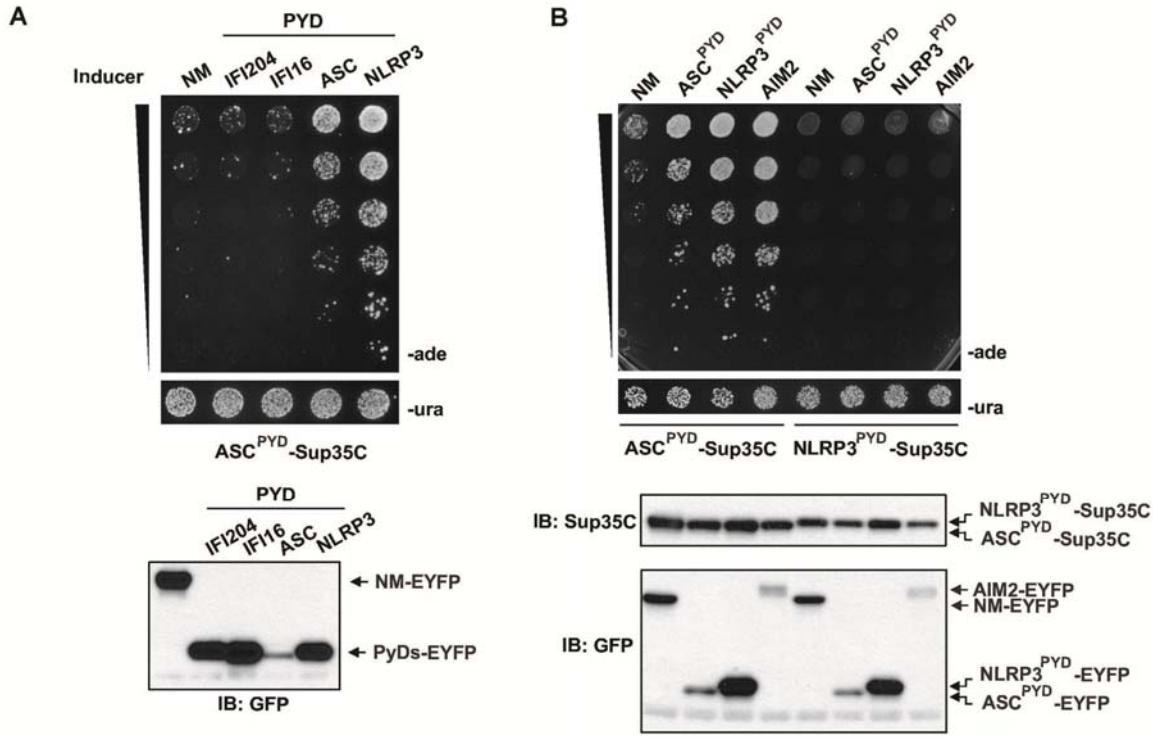


**Figure 13. ASC$^{PYD}$ prion conversion is specific to upstream signals.**

(A) Single colonies with constitutively expressed ASC$^{PYD}$-Sup35C and *GAL* inducible EYFP fusions of NM or PYRIN domains of IF204, IFI16, ASC, and NLRP3 were grown to similar density in SD-ura, followed by incubation in SG-ura for two days. Cells were then plated onto SD-ade and SD-ura at five-fold serial dilutions. Expression of GAL inducible proteins was monitored by a GFP antibody.
(B) Single colonies with constitutively expressed ASC$^{PYD}$-Sup35C or NLRP3$^{PYD}$-Sup35C and *GAL* inducible NM, ASC$^{PYD}$, NLRP3$^{PYD}$, or AIM2$^{FL}$ were grown to similar density in SD-ura, followed by incubation in SG-ura for two days. Cells were then plated as in (E). Expression of GAL inducible proteins was monitored by a GFP antibody. Expression of Sup35 fusions was monitored with a Sup35C antibody.

**ASC$^{PYD}$ Mutants That Disrupt Its Prion Activity Are Defective in Inflammatory Signaling**

ASC$^{PYD}$ shares the same overall six α-helical bundle structure that is the hallmark of the DD superfamily (Ferrao and Wu, 2012). Structural analysis of ASC$^{PYD}$ and NLRP3$^{PYD}$ revealed a strong dipole moment created by adjacent positively and negatively charged surface patches, suggesting that electrostatic interactions may play a role in PYRIN-PRYIN interaction (Liepinsh et al., 2003). Mutations of a number of conserved, surface exposed ASC$^{PYD}$ residues have been shown to be defective in binding to ASC and NLRP3, without affecting protein folding as observed by NMR (Vajjhala et al., 2012). To investigate the consequence of ASC prion formation on its signaling abilities, we tested mutants at several conserved charged and hydrophobic residues (R41A, D48A, and P40A) in our yeast prion assay and for their ability to generate mature caspase-1 and IL-1β in mammalian cells. In yeast, transient NLRP3$^{PYD}$ expression led to the prion conversion of WT and P40A ASC$^{PYD}$, but not R41A or D48A ASC$^{PYD}$ (Figure 14A), suggesting ASC R41A and D48A to be defective in inflammasome signaling.

In 293T cells, The NLRP3 inflammasome pathway has been reconstituted through the exogenous expression of NLRP3, ASC, and pro-caspase-1, components not normally expressed in 293T (Agostini et al., 2004). To test the signal dependent activation of the ASC mutants in cells, we transfected ASC WT or mutants in 293T cells stably expressing NLRP3, pro-caspase-1, and pro-IL-1β, and then subjected the cells to a time course of treatment with Nigericin, a chemical known to strongly activate NLRP3. Inflammasome activation was monitored through the cleavage of pro-caspase-1 and the secretion of caspase-1 (p10) and

IL-1β (p17) into the culture supernatant. Consistent with NLRP3$^{PYD}$ dependent prion conversion in yeast, we observed caspase-1 activation and secretion of p10 and p17 only in ASC WT or P40A expressing cells, while ASC R41A and D48A were defective (Figure 14B).

To investigate the mechanism of the observed signaling defect, we tested homotypic interactions between the WT and mutant ASC$^{PYDs}$, which may be different from its interactions with PYRINs of upstream sensors. To this end, we first examined whether the expression of mutant ASC$^{PYD}$ could induce the prion switch in WT ASC$^{PYD}$-Sup35C cells. Conversely, we also tested whether WT ASC$^{PYD}$ could induce the prion switch in cells containing mutant ASC$^{PYD}$-Sup35C. Interestingly, we found that the mutants behaved similarly in both assays. Namely, ASC$^{PYD}$ R41A and D48A could neither induce prion conversion of WT ASC$^{PYD}$-Sup35C nor could they be induced to form prions themselves (Figures 14C and 14D). P40A behaved similarly to the WT protein in both assays. Western analysis indicated that the expression of the mutants were either at the same level or higher than the WT control. These results suggest that as a part of their respective positive and negative patches, R41 and D48 mediate essential interactions necessary for both the nucleation and polymerization of ASC.

ASC is known to spontaneously activate caspase-1 after *in vitro* incubation when cells expressing both proteins are lysed in a low salt buffer (Martinon et al., 2002). Taking advantage of this *in vitro* ASC-dependent caspase-1 activity assay, we transiently expressed ASC WT, R41A, D48A, and P40A in 293T cells. Lysates from 293T cells expressing ASC and those stably expressing pro-caspase-1 and pro-IL-1β (as assay substrates) were incubated

at 30°C for 45 minutes. Western blot analysis for active subunits of caspase-1 (p10) and IL-1β (p17) indicated that both ASC WT and P40A robustly activated caspase-1 and IL-1β *in vitro*, whereas the R41A and D48A mutants that were defective in prion formation in yeast were also defective in activating caspase-1 and IL-1β (Figure 14E). Collectively, these data demonstrate that ASC mutants unable to form self-perpetuating prions in yeast are also incapable of activating the inflammasome in cells, suggesting that prion formation is necessary for ASC activity.

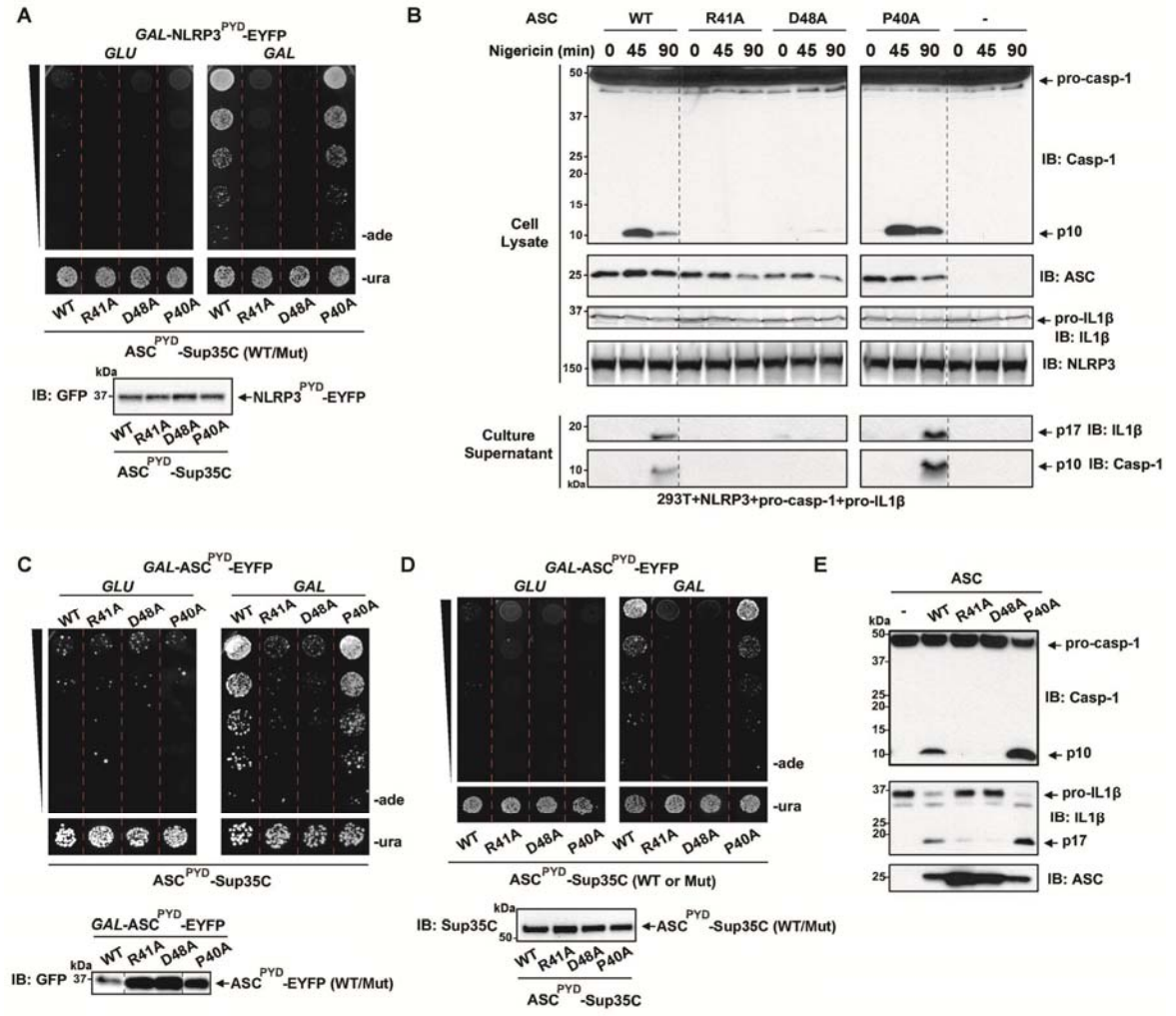


**Figure 14. ASC$^{PYD}$ prion defective mutants are defective in inflammasome signaling.**

(A) Individual yeast colonies constitutively expressing WT or mutant ASC$^{PYD}$-Sup35C and *GAL*-NLRP3$^{PYD}$-EYFP were grown in SD-ura or SG-ura for two days, followed by plating of five-fold serial dilutions onto SD-ura and SD-ade.
(B) Nigericin was added to ASC WT or mutant transfected 293T cells stably expressing NLRP3, pro-caspase-1, and pro-IL-1β, followed by western blot analysis of cell lysates for caspase-1 processing and of culture supernatants for active caspase-1 (p10) and IL-1β (p17) secretion.
(C) Similar to (A), except that WT or mutant ASC$^{PYD}$, instead of NLRP3$^{PYD}$, was used to induce ASC$^{PYD}$ prion conversion.
(D) Individual colonies constitutively expressing WT or mutant ASC$^{PYD}$-Sup35C and WT *GAL*-ASC$^{PYD}$-EYFP were treated as in (A).
(E) Lysates of 293T cells expressing WT or mutant ASC were incubated with pro-caspase-1 and pro-IL-1β containing cell extracts, followed by analysis of caspase-1 and IL-1β cleavage by western blotting. Irrelevant lanes were removed for clarity.

**Reconstitution of Inflammasome Signaling in Yeast Reveals Caspase-1 Activation Only in Colonies with ASC Prion Particles**

Next, we sought to determine if prion conversion of full-length ASC ($ASC^{FL}$) could be recapitulated in our yeast assay. We generated a strain of yeast expressing $ASC^{FL}$-Sup35C in place of endogenous Sup35, and tested for prion conversion after transient expression of $AIM2^{FL}$, $NLRP3^{PYD}$, and WT or mutant $ASC^{PYD}$. $AIM2^{FL}$ and $NLRP3^{PYD}$ induced a >200-fold increase in Ade+ colonies on SD-ade and the appearance of white colonies on ¼YPD (Figures 15A and 5B). Moreover, $ASC^{PYD}$ mutants that were defective in prion formation were also defective in the context of full-length ASC (Figure 15A; 16A, B). SDD-AGE analysis revealed that $ASC^{FL}$-Sup35C had acquired SDS-resistant polymers in the Ade+ isolates (designated [$ASC^{FL}$+]), but not in the ade- isolates (designated [$asc^{fl}$-]) (Figure 15C). These results indicate that AIM2 and NLRP3 induced $ASC^{FL}$ to convert to a self-perpetuating prion form.

We then applied our phenotypic assay to test if caspase-1 and NLRC4, which harbor N-terminal CARDs but no PYRIN domains, could induce the ASC prion switch. As an important inflammasome sensor for bacterial flagellin and type III secretion systems, NLRC4 can directly activate caspase-1, but this activity is markedly enhanced in the presence of ASC (Atianand et al., 2013; Broz et al., 2010). When expressed in yeast, a C284A active site mutant caspase-1 was unable to induce ASC (PYRIN, CARD, or full length)-Sup35C yeast to form Ade+ colonies (Figure 17A). However, expression of $NLRC4^{CARD}$ induced $ASC^{FL}$-Sup35C but not $ASC^{PYD}$- or $ASC^{CARD}$-Sup35C prion conversion, and this effect was abolished in yeast harboring $ASC^{FL}$-Sup35C R41A or D48A polymerization mutants (Figure

17B). These results suggest that NLRC4$^{CARD}$ is able to activate ASC$^{FL}$ through CARD-CARD interactions, but this activation is strictly dependent on ASC$^{PYD}$ mediated polymerization. Despite its ability to also interact with ASC$^{CARD}$, caspase-1 cannot induce ASC$^{FL}$ polymerization.

To test whether the ASC$^{FL}$-Sup35C fusion could function in inflammasome signaling, we transfected ASC$^{FL}$-Sup35C into 293T cells stably expressing NLRP3, pro-caspase-1 and pro-IL-1β. Following a time course of Nigericin treatment, caspase-1 cleavage was observed and secretion of p10 and p17 was detected in the culture supernatant, suggesting that the ASC$^{FL}$-Sup35C retains the inflammasome signaling activity of WT ASC (Figure 18). Next, to reconstitute caspase-1 activation in yeast, cells harboring ASC$^{FL}$-Sup35C were transformed with constitutively expressed pro-caspase-1 along with galactose-inducible AIM2$^{FL}$ or NLRP3$^{PYD}$ (Figure 19A). Transient expression of either AIM2$^{FL}$ or NLRP3$^{PYD}$ led to the appearance of white colonies on ¼YPD similar to those observed in yeast without caspase-1 (data not shown). Further passaging of these colonies revealed an appreciable rate of switching back to the red phenotype, indicative of a bistable, epigenetically inherited trait (Figure 19B). We then used a colony lysis procedure to assess caspase-1 activation in individual colonies (Kushnirov, 2000). Strikingly, we observed pro-caspase-1 cleavage only in [*ASC*$^{FL}$+] but not [*asc*$^{fl}$-] colonies, despite their having originated from the same [*ASC*$^{FL}$+] colony (Figure 19C). Altogether, these results strongly suggest that ASC prion formation and propagation is necessary and sufficient for downstream signaling.

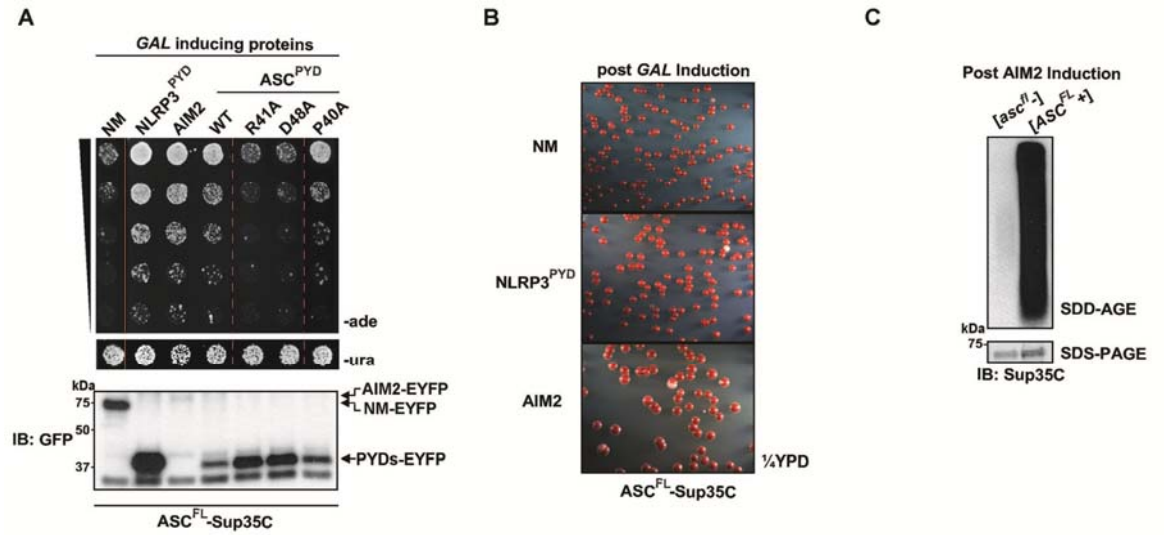


**Figure 15. ASC$^{FL}$ is a prion in yeast.**

(A) Single colonies with constitutively expressed ASC$^{FL}$-Sup35C and *GAL* inducible NM, NLRP3$^{PYD}$, AIM2$^{FL}$, WT or mutant ASC$^{PYD}$ were grown to similar density in SD-ura, followed by incubation in SG-ura for two days. Five-fold serial dilutions were then plated onto SD-ade and SD-ura. Expression of GAL inducible proteins was monitored by a GFP antibody.
(B) Similar to (A) except that cells were plated to ¼YPD at 500 cells/plate.
(C) Following induction of Ade+ by AIM2$^{FL}$ expression, colonies with soluble or prion form of ASC$^{FL}$-Sup35C ([*asc$^{fl}$*-] or [*ASC$^{FL}$*+], respectively) were subjected to SDD-AGE analysis for SDS-resistant aggregates and SDS-PAGE for expression levels.

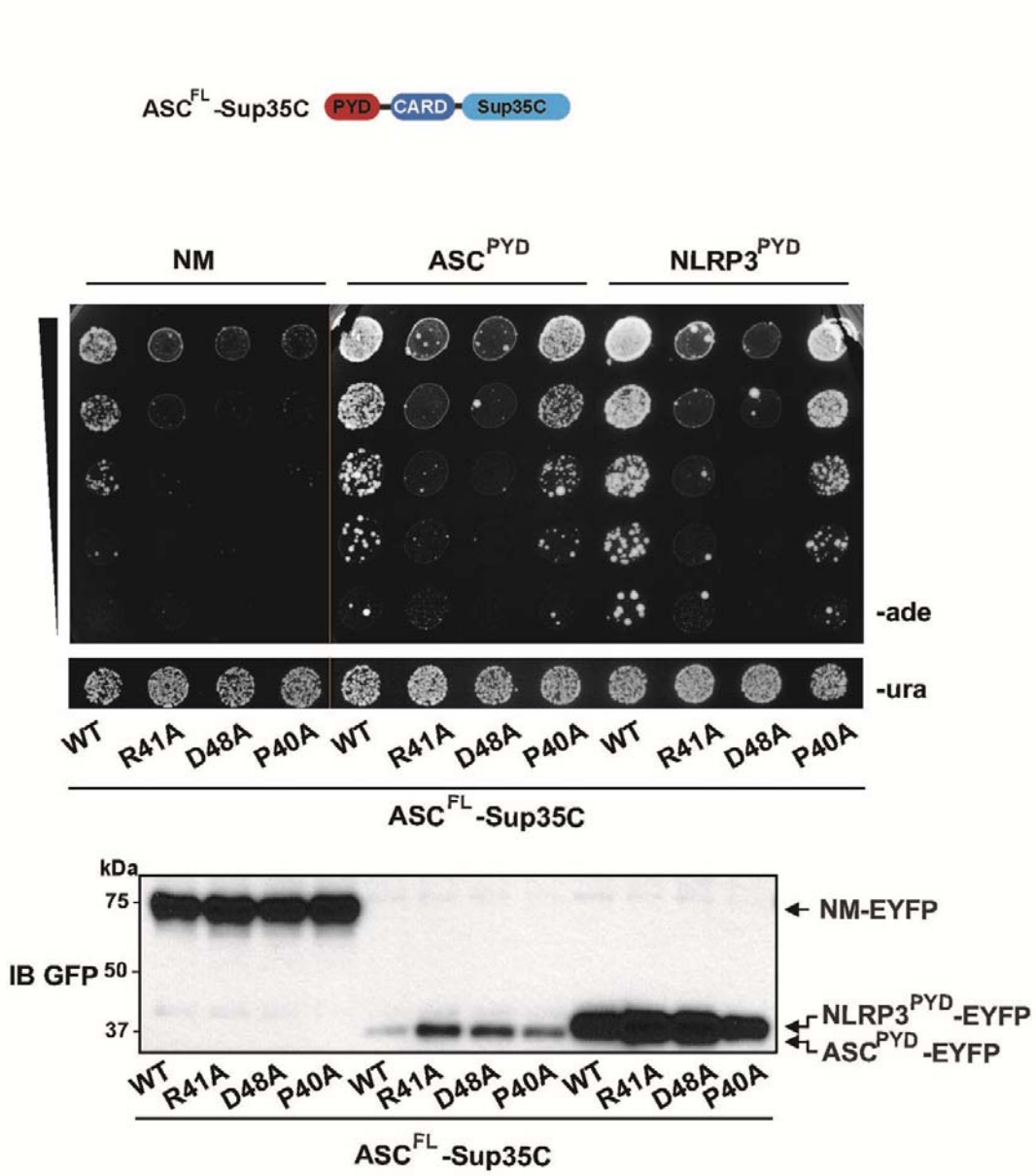


**Figure 16. ASC$^{FL}$ mutants are defective in prion conversion.**

(A) Domain organization of ASC$^{FL}$-Sup35C.
(B) Single colonies with constitutively expressed WT or mutant ASC$^{FL}$-Sup35C and *GAL* inducible NM, ASC$^{PYD}$ or NLRP3$^{PYD}$ were grown to similar density in SD-ura, followed by incubation in SG-ura for two days. Cells were then plated onto SD-ade and SD-ura at five-fold serial dilutions. Expression of GAL inducible proteins was monitored by a GFP antibody.

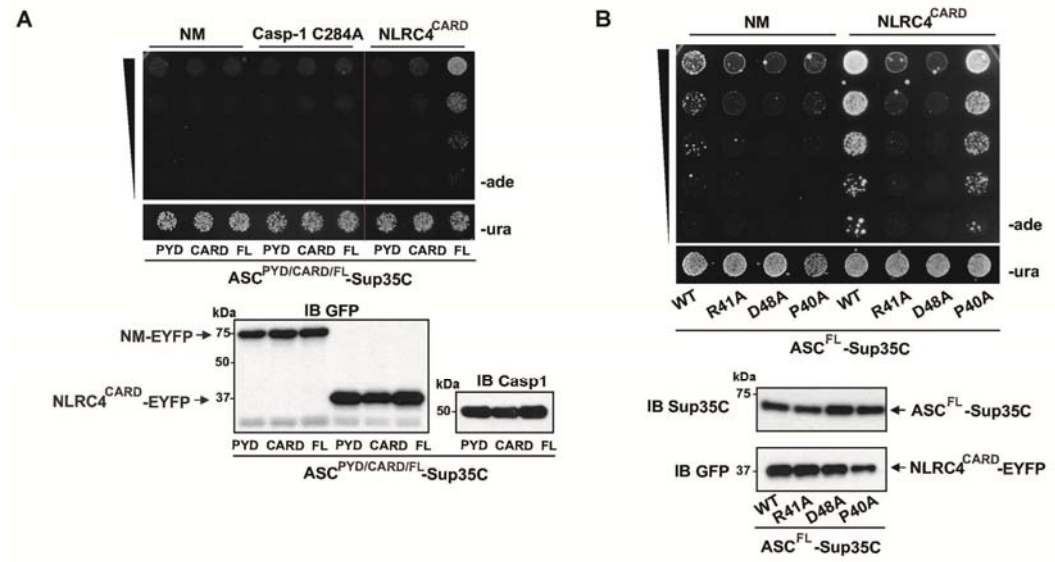


**Figure 17. NLRC4$^{CARD}$ can induce ASC prion conversion in yeast.**

(A) Similar to (16B), except yeast harboring Sup35C fusions to full-length or different domains of ASC were used. The *GAL* inducible proteins included the catalytically inactive mutant of caspase-1 (Casp-1 C284A) and NLRC4 CARD domain.
(B) Similar to (16B), except that yeast harboring *GAL* inducible NLRC4$^{CARD}$ were used.

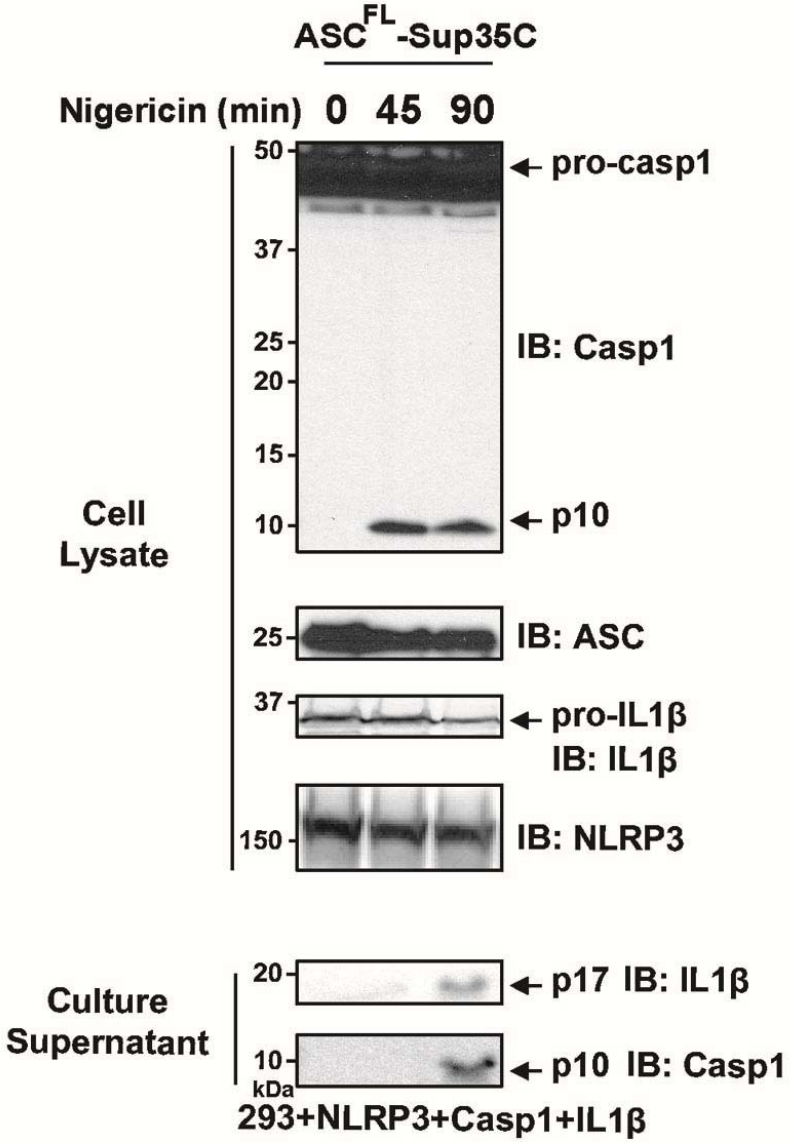


**Figure 18. NLRC4$^{CARD}$ can induce ASC prion conversion in yeast.**

ASC$^{FL}$-Sup35C was transiently transfected into 293T cells stably expressing NLRP3, pro-caspase-1 and pro-IL-1□ (293T+NLRP3+Caspase-1+ IL-1β). Eighteen hours later, nigericin (10μM) was added and inflammasome signaling was followed by western blotting of culture supernatants for mature caspase-1 (p10) and IL-1β (p17) secretion. Expression of NLRP3, IL-1β, ASC$^{FL}$-Sup35C, and caspase-1 in the cell lysates was monitored with their respective antibodies.

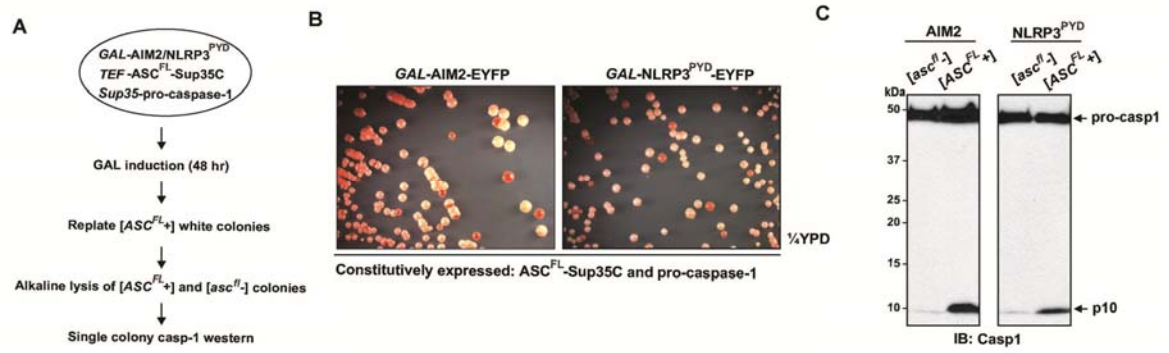


**Figure 19. Only cells with ASC$^{FL}$ prion particle activates caspase-1.**

(A-C) Schematic for the reconstitution of inflammasome signaling in yeast (A). Yeasts expressing AIM2$^{FL}$- or NLRP3$^{PYD}$-EYFP from a *GAL* inducible promoter (Ura+), ASC$^{FL}$-Sup35C from the constitutive *TEF* promoter, and pro-caspase-1 from the constitutive *SUP35* promoter were grown in galactose containing media for 2 days. The resultant [*ASC*$^{FL}$+] colonies were re-streaked onto ¼YPD (B), from which individual *[asc*$^{fl}$*-]* or [*ASC*$^{FL}$+] colonies were lysed and subjected to western analysis for caspase-1 activation (C).

**Recombinant ASC$^{PYD}$ Fibers Converts Inactive ASC into a High Molecular Weight Form Capable of Downstream Signaling**

Mammalian PrP and known yeast prions typically adopt fibrous structures that perpetuate protein-based forms of inheritance by undergoing cycles of seeding, polymerization, and fragmentation (Toyama and Weissman, 2011). To investigate whether the prion domain of ASC exhibits similar properties, ASC$^{PYD}$ (N1-90) was expressed in *E. coli.* and purified under native conditions to apparent homogeneity. The protein eluted in one peak at the void volume (>700kDa) on Superdex-200 gel filtration chromatography. Negative-stain electron microscopy analysis of the protein revealed that ASC$^{PYD}$ assembled into fibers with an electron poor center, suggestive of symmetry about a central axis (i.e. rotational symmetry) (Figure 20A).

The defining property of prions is an ability to convert native species of the protein into a polymerized, infectious form (Prusiner, 1998). To determine if ASC$^{PYD}$ fibers can induce a similar switch to native ASC protein, we first sought conditions that would separate polymerized form of ASC from its native form. Previous work has shown that upon activation, ASC forms a distinct focus in cells and also shifts to high molecular weight fractions on gel filtration chromatography (Broz et al., 2010; Jones et al., 2010; Martinon et al., 2002). Using a sucrose density gradient, we fractionated lysate from 293T cells stably expressing NLRP3 and ASC$^{FL}$-GFP before and after Nigericin treatment. Nigericin treatment resulted in the formation of large ASC$^{FL}$ particles that sedimented to the bottom of a 20%-60% sucrose gradient (Figure 20B, top). When incubated with lysate from 293T cells stably expressing pro-caspase-1, only the high molecular weight fractions were capable of

activating caspase-1, suggesting that the active form of $ASC^{FL}$ consists of large $ASC^{FL}$ particles (Figure 20B, bottom). We then incubated a sub-stoichiometric amount of $ASC^{PYD}$ fibers with $ASC^{FL}$-GFP (~1:10,000 molar ratio) and observed a notable shift of $ASC^{FL}$ from a low molecular weight to a high molecular weight form that also sedimented to the bottom of the sucrose gradient (Figure 20C, top). An in vitro assay revealed that only the high molecular weight fractions were capable of activating caspase-1 (Figure 20C, bottom). These results indicate that $ASC^{PYD}$ fibers converted native ASC into an active, self-perpetuating, and high molecular weight polymer similar to the one induced by activated NLRP3 in vivo.

To further demonstrate the infectious properties of $ASC^{PYD}$ fibers, we incubated sub-stoichiometric amounts of $ASC^{PYD}$ fibers with lysates from 293T cells expressing $ASC^{FL}$-GFP, which is not active by itself, at 30°C for 60 minutes. All reactions were supplemented with lysate from 293T cells stably expressing pro-caspase-1 as the substrate. Western blot analysis revealed that only the combination of $ASC^{PYD}$ fibers with $ASC^{FL}$-GFP, but not either one alone, resulted in caspase-1 activation (Figure 21A and 21B). Titration experiments showed that incubation of less than 0.2 ng of $ASC^{PYD}$ fibers with ~5 □g of $ASC^{FL}$-GFP led to detectable cleavage of pro-caspase-1. In contrast, incubation of 500 ng of NM fibers with ~5 □g $ASC^{FL}$-GFP failed to activate caspase-1. Taken together, these results suggest that a catalytic and self-perpetuating polymerization of ASC governs inflammasome activation.

To examine the consequence of ASC polymerization on downstream signaling, we probed the interaction between ASC and pro-capase-1 following AIM2 transfection, which activates the inflammasome (Fernandes-Alnemri et al., 2009; Hornung et al., 2009). In lysate from 293T cells stably expressing flag-caspase-1 C284A and ASC-GFP WT or R41A, GFP

immunoprecipitation revealed that only ASC-GFP WT but not R41A was able to interact with pro-caspase-1 in an Aim2 dependent manner (Figure 22A). Furthermore, sucrose gradient analysis indicated that following AIM2 stimulation, only ASC-GFP WT, but not R41A, formed high molecular weight particles, which recruited pro-caspase-1 (Figure 22B).

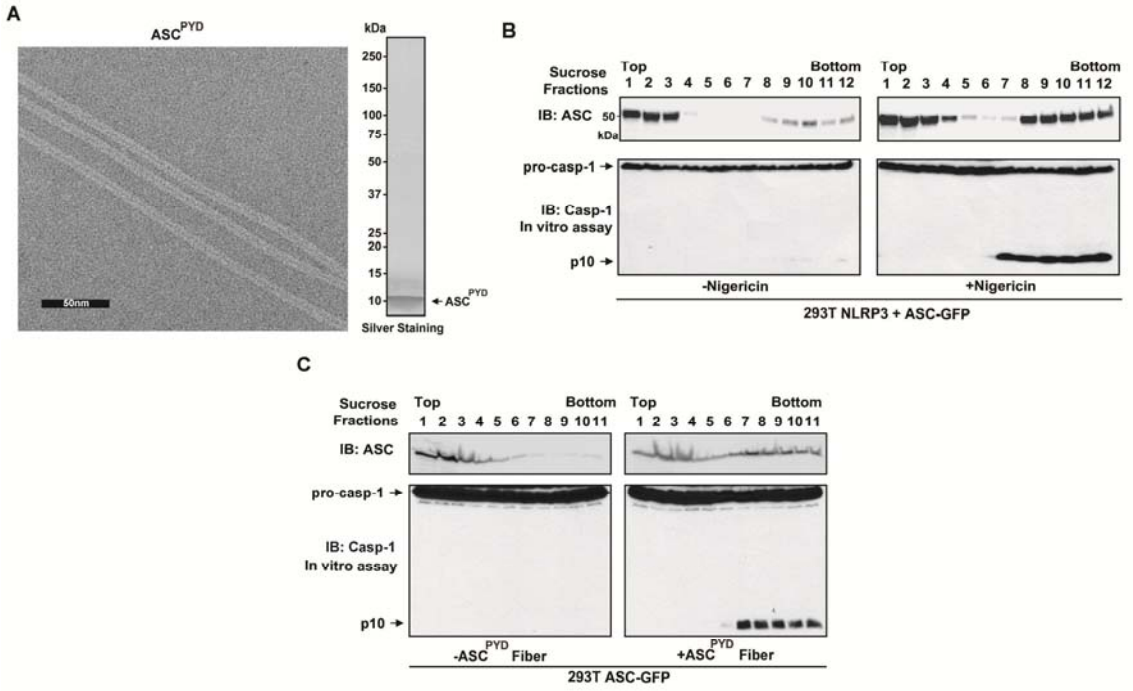


**Figure 20. ASC fibers convert ASC into functional aggregates.**

(A) Electron microscopy of negatively stained recombinant $ASC^{PYD}$ purified to apparent homogeneity, as indicated by silver staining. (Performed by Hui Xu)
(B) 293T cells stably expressing NLRP3 and $ASC^{FL}$-GFP were fractionated on a 20-60% sucrose gradient cushion for two hours at 170,000g before and after Nigericin treatment for 60 minutes. Individual fractions were western blotted with an ASC specific antibody (top) or incubated with extract from 293T cells stably expressing pro-caspase1 (as assay substrate) at 30°C for 60 minutes, followed by western analysis of caspase-1 activation.
(C) Lysate from 293T cells stably expressing $ASC^{FL}$-GFP were incubated at 30°C for 30 minutes with or without $ASC^{PYD}$ fibers, followed by the same analysis as in (B).

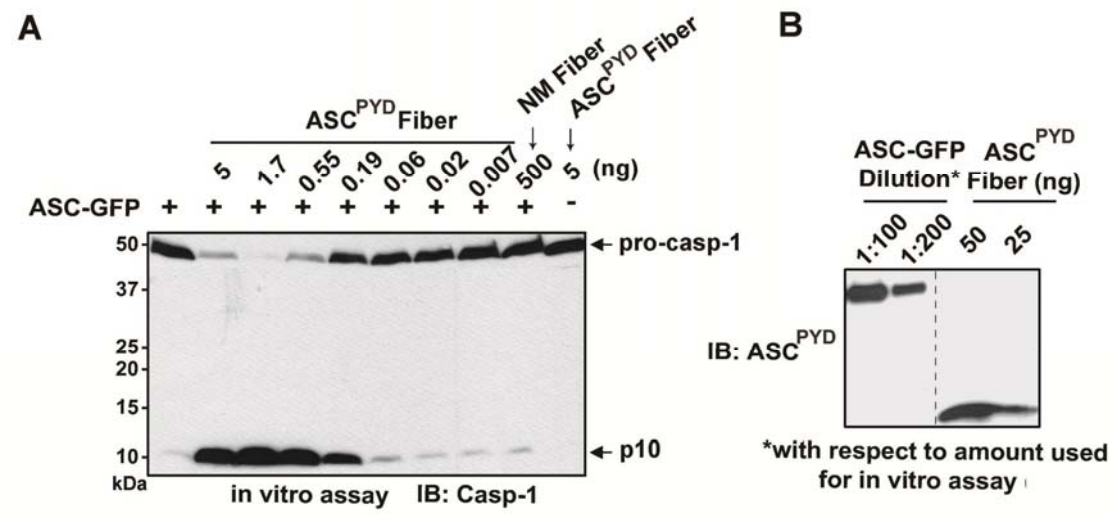


**Figure 21. ASC fibers convert ASC into functional aggregates.**

(A) Lysates from 293T cells stably expressing $ASC^{FL}$-GFP were incubated at 30°C for 60 minutes with different amounts of $ASC^{PYD}$ fibers or NM fibers as indicated, along with extract from 293T cells stably expressing pro-caspase-1 (as assay substrate), followed by western analysis for caspase-1 activation. The last lane does not contain $ASC^{FL}$-GFP. (B) Dilutions of lysate of 293T cells stably expressing $ASC^{FL}$-GFP as in (D) was quantitatively compared to different amounts of $ASC^{PYD}$ fibers by western blotting with an antibody specific to $ASC^{PYD}$.

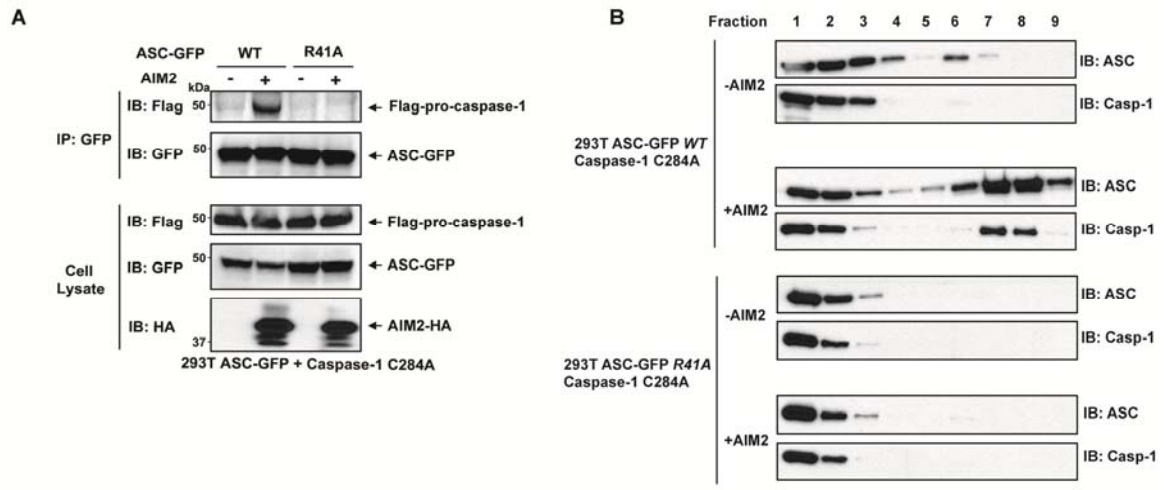


**Figure 22. ASC aggregates recruit caspase-1.**

(A) 293T cells stably expressing Flag-caspase-1 C284A and ASC-GFP WT or R41A were transfected with an AIM2 expression plasmid or mock treated. ASC was immunoprecipitated with a GFP antibody and then co-immunoprecipitated Flag-caspase-1 was immunoblotted with a Flag antibody.
(B) Lysate from (F) was fractionated on a 20-60% sucrose gradient cushion followed by immunoblot analysis of each fraction with indicated antibodies.

**A Conserved Fungal Pattern Recognition Receptor and Death Inducing Prion Functionally Replace NLRP3$^{PYD}$ and ASC$^{PYD}$ in Inflammasome Signaling**

In addition to Sup35, there are a number of other well characterized fungal prions, of which HET-s from the filamentous fungus *Podospora anserina* shares notable similarities with MAVS and ASC. Unlike yeast prions, the prion form of HET-s functions strictly in a gain-of-function manner that induces cell death. Also unlike yeast prions, it does not require Hsp104, and the prion fibers fail to stain with the amyloid-binding dye Thioflavin T (ThT) (Saupe, 2011). Similarly, MAVS and ASC also switch into gain-of-function prions which propagate independently of Hsp104 in yeast, because inactivation of Hsp104 by 3 mM guanidine hydrochloride (GnHCl) (Ness et al., 2002), which converted [*PSI*+] into [*psi*-] state, did not cause [$ASC^{PYD}$+] or [$MAVS^{CARD}$+] prion to convert into the soluble forms (Figure 23A). The recombinant fibers of their prion domains also do not stain with ThT, suggesting they do not form prototypical β-amyloids (Figure 23B).

In filamentous fungi, spontaneous cell fusion leads to cell death only if one partner expresses HET-S, and the other harbors the prion form of HET-s ([*HET-s*]), an allelic variant of HET-S that shares the same prion domain. Specifically, upon cell fusion, [*HET-s*] templates prion-like conversion of HET-S, which leads to a conformational change in the HET-S HeLo domain that converts it into a pore-forming toxin (Seuring et al., 2012). However, in the presence of soluble (non-prion) HET-s, HET-S does not cause cell death. The hypothesis that HET-s/S serves host defense functions is supported by a recent bioinformatics analysis that discovered that NWD2, encoded by a gene adjacent to the HET-s/S locus, closely resembles

mammalian NOD-like receptors (NLR) such as NLRP3, and may function as a signaling partner of HET-s/S (Daskalov et al., 2012). Similar to NOD-like receptors, NWD2 harbors a C-terminal WD40 repeat, a middle NACHT (or nucleotide-binding oligomerization) domain, and an N-terminal domain predicted to homologous to the Het-s/S prion domain. Overall, the fungal NWD2 and HET-s pair is strikingly similar to mammalian NLRP3 and ASC, both in terms of organization and function (Figure 24A).

To determine if NWD2 can induce HET-s polymerization, and if the NWD2/HET-s pair is a possible fungal counterpart to NLRP3 and ASC, we tested if the NWD2 N-terminal domain ($NWD2^{N30}$) and HET-s prion domain ($HET\text{-}s^{PrD}$) can reconstitute inflammasome signaling (Figure 24B). After replacing $ASC^{PYD}$ with $HET\text{-}s^{PrD}$, we stably expressed the fusion protein with a C-terminal EYFP tag in 293T cells. We observed that $HET\text{-}s^{PrD}$-$ASC^{\Delta PYD}$-EYFP was distributed diffusely throughout the cell. The localization pattern did not change with the co-expression of $NWD2^{N50}$ (to facilitate western blot analysis) or NLRP3 (Figure 7C). However, co-expression of $NWD2^{N30}$-$NLRP3^{\Delta PYD}$ ($NLRP3^{PYD}$ replaced by $NWD2^{N30}$) resulted in a striking redistribution of $HET\text{-}s^{PrD}$-$ASC^{\Delta PYD}$-EYFP to form a single perinuclear focus in almost every cell, reminiscent of the previously described ASC foci (Figure 24C). These results suggest that $NWD2^{N30}$ is necessary but not sufficient for $HET\text{-}s^{PrD}$-$ASC^{\Delta PYD}$ prion conversion, and suggest that the NACHT domain of NWD2 is required for its oligomerization and downstream signaling, similar to the current model for NLRP3 activation. Next, we generated cell lines stably expressing NLRP3 or $NWD2^{N30}$-$NLRP3^{\Delta PYD}$ along with pro-capase-1 and pro-IL1β and transfected either WT ASC or $HET\text{-}s^{PrD}$-$ASC^{\Delta PYD}$

into the two cell lines. Nigericin treatment revealed that mature IL1β (p17) was only secreted in cells expressing WT NLRP3 and ASC or NWD2$^{N30}$-NLRP3$^{\Delta PYD}$ and HET-s$^{PrD}$-ASC$^{\Delta PYD}$, indicating that each receptor specifically interacts with its cognate prion (Figure 24D). Together, these results suggest that fungi possess a programmed cell death pathway that is mechanistically similar to those in mammals (Figure 25). Furthermore, the regulated conversion of prion domain containing proteins (Het-s/S and ASC) into their prion forms by pattern recognition receptors (e.g., NWD2 and NLRP3) is an evolutionarily conserved mechanism of signal transduction from fungi to mammals.

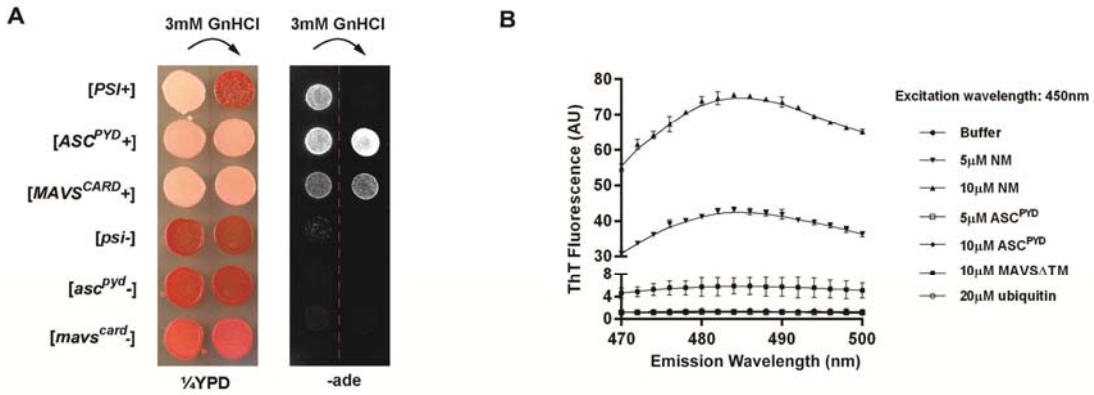


**Figure 23. MAVS and ASC have atypical prion behavior.**

(A) Yeast strains harboring the indicated prion states were plated on ¼YPD or SD-ade following serial passages on plates containing 3mM GnHCl, which inactivates Hsp104 and therefore eliminates Hsp104-dependent prion states.
(B) Emission spectra of thioflavin T (ThT), a dye that fluoresces upon binding to amyloid, in the presence of the indicated recombinant proteins. ThT was excited at 450nm

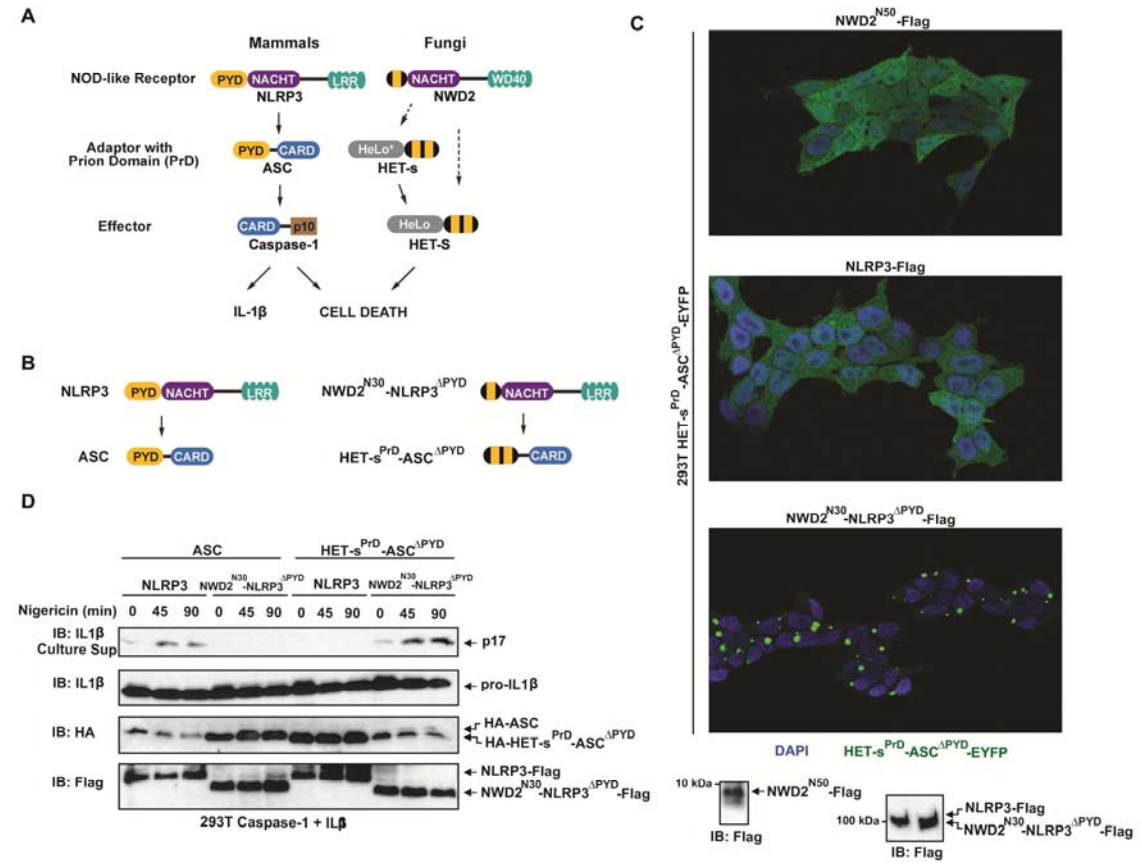


**Figure 24. NWD2 activates HET-S.**

(A) Cartoon representations of the mammalian NLRP3 inflammasome signaling and fungal NWD2 signaling pathways. Dotted arrow indicates an unconfirmed potential signaling interaction. The predicted HET-s$^{PrD}$ fold of NWD2 N-terminal domain is indicated using a yellow stripe, whereas HET-s$^{PrD}$ harbors two such motifs in tandem. Asterisk indicates inactive HeLo domain.
(B) Cartoon representations of fusion proteins between NWD2/HET-s and NLRP3/ASC.
(C) Confocal microscopy images of 293T cells stably expressing HET-s$^{PrD}$-ASC$^{\Delta PYD}$-EYFP and transfected NWD2$^{N50}$, NLRP3, or NWD2$^{N30}$-NLRP3$^{\Delta PYD}$ as indicated on the top of each image.
(D) 293T cells stably expressing NLRP3 or NWD2$^{N30}$-NLRP3$^{\Delta PYD}$ along with pro-caspase-1 and pro-IL1β were transfected with either WT ASC or HET-s$^{PrD}$-ASC$^{\Delta PYD}$. Following a time course of Nigericin treatment, secretion of mature IL1β and expression of indicated proteins were analyzed by western blotting.

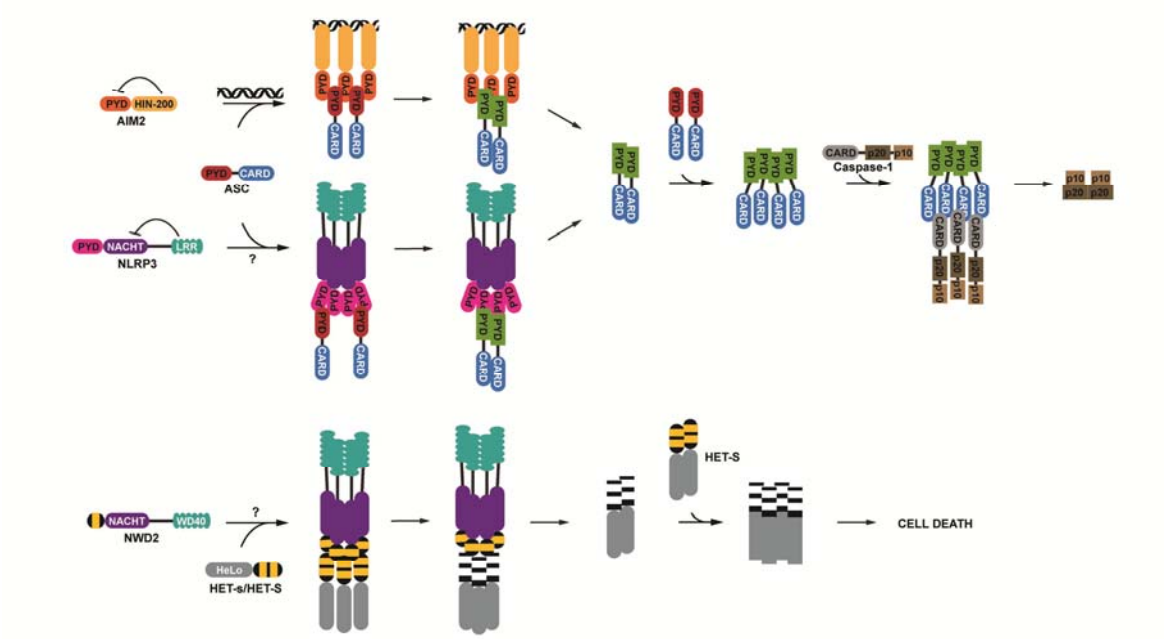


**Figure 25. Model for ASC and HET-s/S signaling.**

Model for ASC-dependent inflammasome signaling. Stimulation by DNA and unknown factor(s) releases the auto-inhibition of AIM2 and NLRP3 respectively, which results in the oligomerization of AIM2 and NLRP3 through their respective HIN200 and NACHT domains and the recruitment of multiple ASC proteins through PYRIN-PYRIN interactions. $ASC^{PYD}$ is converted into a prion-form (depicted as green rectangles) either through direct templating by $AIM2^{PYD}$ or $NLRP3^{PYD}$ or as a result of the close apposition of numerous $ASC^{PYDs}$. The prion form of ASC then templates other, soluble ASC proteins into the prion form, resulting in large, fibrous, self-perpetuating polymers that expose multiple $ASC^{CARDs}$ for binding to downstream caspase-1 through CARD-CARD interactions. Caspase-1 is then activated and cleaves itself, among other substrates.

Model for NWD2 mediated HET-S activation. Following binding of its WD40 repeats to a putative ligand, NWD2 oligomerizes through its NACHT domain causing its N-terminal region to take on a $HET\text{-}s^{PrD}$-like fold, which subsequently nucleates HET-S prion conversion. The prion form of HET-S then templates other soluble HET-S proteins into the prion form (depicted as rectangles with white stripes), which induces structural changes in the HET-S HeLo domain (depicted as rectangles) that turns the protein into a pore-forming membrane toxin. Alternatively, following cell fusion, HET-S prion conversion and toxicity can be templated by the prion form of HET-s, which may be induced by activated NWD2.

# SECTION III

# DISCUSSION

In this report, we provide biochemical and genetic evidence demonstrating that in response to upstream signals, two death domain-containing proteins, MAVS and ASC, each switch into a prion-like form that is necessary and sufficient for downstream signal transduction. MAVS and ASC exhibit hallmarks of prions in yeast, and prion conversion was inducible by their respective upstream signaling proteins (Figure 25, 26). Based on previously published results and those presented here, we propose the following model for ASC mediated inflammasome signaling: (1) Stimulation of NLRP3 or AIM2 induces a conformational change that results in the oligomerization or close apposition of their individual PYRIN domains. (2) These oligomers, through PYRIN-PYRIN interactions, then recruit multiple ASC proteins resulting in prion nucleation, which is otherwise prevented from occurring spontaneously due to a high-energy barrier. (3) ASC prions then rapidly template other ASC molecules resulting in the formation of large polymers. (4) Through CARD-CARD interactions, the ASC polymers recruit multiple caspase-1 molecules, bringing them into close proximity to induce their auto-cleavage and activation (Figure 25). Such a mechanism enables the surveillance system to respond with high sensitivity to foreign pathogens and danger signals to trigger a robust, digital inflammatory response.

The mechanism of NWD2 mediated HET-s/S activation in fungi likely resembles that of NLRP3 mediated ASC and caspase-1 activation in mammals (Figure 25). Following ligand binding to its WD40 repeats, NWD2 oligomerization through its NACHT domain induces its N-terminal region to form a β-solenoid fold, which in turn templates HET-S into a

prion form that converts the HeLo domain into a pore-forming toxin. Alternatively, in cells expressing the allelic variant HET-s, NWD2 activation induces stable prion formation because HET-s contains an inactive HeLo domain, resulting in a decoupling of prion formation from cell death. Nevertheless, when [*HET-s*] cells fuse with cells expressing HET-S, the prion then templates HET-S into the toxic form, leading to death of the fused cell.

**Prion-like Polymerization Is a Sensitive and Robust Mechanism of Cell Signaling**

Our cells are constantly bombarded by an array of extra- and intra-cellular signals and must evolve mechanisms to properly control signal transduction, minimizing noise while responding quickly to urgent calls. In this regard, innate immune signaling is critical for our protection and survival. Studies have shown that deficiency in either the MAVS dependent antiviral or the ASC dependent inflammasome pathway greatly compromises the host, suggesting their signaling is important for host defense. Intriguingly, virus infection and inflammatory signaling are usually detrimental to the affected cell, often resulting in cell death, which protects the host from further damage. The evolution of irreversible signaling mechanisms through prion switches therefore benefits the organism as a whole at the expense of individual cells.

While other signaling amplification mechanisms exist (i.e. the formation of defined, cooperative oligomeric complexes that bring signaling components into proximity), a self-perpetuating mechanism of signal amplification in response to a stimulation threshold ensures an irreversible commitment to the appropriate response. This ultrasensitive mechanism is also in line with our previous estimate that as few as 20 viral RNA molecules

are capable of activating the RIG-I antiviral signaling cascade, suggesting autocatalytic signal propagation that only requires a brief stimulus to turn on (Zeng et al., 2010). Furthermore, signal transduction through the formation of fibrous particles offers cells not only temporal, but also spatial control over signal transduction. Notably, activated MAVS and ASC both form distinct punctate structures in cells and sediment to high molecular weight fractions in sucrose gradients. Interestingly, recent work has implicated MAVS in the subcellular localization of the NLRP3 inflammasome (Subramanian et al., 2013). Consistent with the idea that these prion polymers serve as signalosomes for recruitment of downstream signaling molecules, we recently showed that mutations abolishing MAVS aggregation prevented the recruitment of TRAF proteins necessary for signal propagation, essentially harboring the same deficiency of *Mavs*$^{-/-}$ cells in the response to viral infection (Liu et al., 2013).

MAVS and ASC share similarities in their function (as innate immune adapters) and overall structure (as DD superfamily members), but their signaling through prion conversion may not be unique. For example, a recent bioinformatics analysis suggested the existence of other NLR and prion protein pairs across the fungal kingdom, indicating an evolutionary conserved mechanism of signal transduction (Daskalov et al., 2012). Moreover, studies have indicated that proteins in necrosis signaling (RIP1/3) and NF-κB activation (CARMA1 and Bcl10) also form large oligomers or even fibers, though it remains to be seen if they undergo prion-like self-perpetuation (Li et al., 2012; Qiao et al., 2013; Sun et al., 2004). Interestingly, in the course of screening other DDs for possible prion conversion, we observed spontaneous prion-like switching of RIP1$^{DD}$ that warrants further investigation.

The properties of MAVS and ASC distinguish them from non-prion polymer-forming proteins. The soluble forms of prion proteins are energetically less stable than their corresponding polymeric forms, and are separated from these forms merely by the high energy of nucleation. Under normal conditions, the "native", inactive states predominate because they are kinetically trapped. Factors that stimulate prion formation, such as the [*PIN*+] prion in the case of Sup35 and upstream signaling proteins (RIG-I, AIM2, NLRP3, and NLRC4) in the cases of MAVS and ASC, do so by lowering the energy of nucleation. Once nucleation has been achieved, energetically downhill and thus irreversible polymerization ensues. The prion states subsequently perpetuate independently of the nucleating factors. Hence, a population is characterized by a bi-modal distribution of cells that each contains either the native or prion form of the protein. In contrast, polymerization of non-prion proteins is dynamic and reversible, and the distribution between soluble and polymeric forms is typically regulated by changes in their relative stabilities. The polymerization of actin and tubulin, for example, are each regulated by nucleotide (ATP and GTP, respectively) binding and hydrolysis. Here, the soluble and polymerized forms of a protein are uniformly distributed within an individual cell and a population.

Likewise, not all proteins that form oligomers are capable of forming self-perpetuating polymers. For example, in Toll-like receptor signaling, the adapter MyD88 forms a finite but ordered helical structure known as the Myddosome that includes the protein kinases IRAK4 and IRAK2 (Lin et al., 2010). For caspase-2 activation, upstream proteins PIDD and RAIDD also form a fixed complex named the Piddosome that is composed of seven RAIDD DDs and five PIDD DDs, which then recruit and activate

caspase-2 (Park et al., 2007b). The structural and biophysical differences that cause some DD superfamily members to form open-ended polymers and others to form limited oligomers remain to be elucidated.

**Unique Features of MAVS and ASC as Prion-like Proteins**

Since the "prion hypothesis" was first proposed more than two decades ago, we have come to understand prions not only as causative agents of debilitating diseases, but also as potentially adaptive mechanisms for phenotypic diversification and information storage (Holmes et al., 2013; Prusiner, 1982; Si et al., 2010; True and Lindquist, 2000). In yeast, over a dozen prion-like proteins have been discovered. With few exceptions, most possess prion domains that are natively disordered and enriched in glutamines (Q) and/or asparagines (N) (Liebman and Chernoff, 2012; Suzuki et al., 2012). The prion forms of these proteins can exert wide-spread phenotypic effects that may be advantageous in the face of fluctuating environments (Alberti et al., 2009; Halfmann et al., 2012; Tuite and Serio, 2010). In *Aplysia* and *Drosophila* a neuronal translation regulator, CPEB, forms multimers that appear to maintain long-term memory through prion-like self-perpetuation (Majumdar et al., 2012b; Si et al., 2010). In contrast, prior to the discovery of MAVS as a prion, beneficial prions were not known to exist in mammals, where the first prion was discovered.

Here we show that MAVS and ASC are two mammalian proteins capable of switching into functional prions, which differ from previously described prions in several important aspects. First, the prion domains of both proteins are neither intrinsically disordered nor rich in Q and N amino acids. Rather, they adopt well-folded six α-helical

bundle structures (Liepinsh et al., 2003; Potter et al., 2008). The detergent-resistant filaments of MAVS and ASC do not appear to be amyloid-like, as they do not react with ThT. Secondly, while most prions display loss-of-function phenotypes, the prion forms of MAVS and ASC signal in a gain-of-function manner. Mutations that abolish their prion activities also abrogate their biological functions. Thirdly, nearly all previously described prion proteins acquire their prion forms in a stochastic or semi-stochastic manner. MAVS and ASC, on the other hand, undergo stimulus-dependent prion conversion that is contingent on heterotypic interactions with upstream protein sensors. In other words, the nucleation of MAVS and ASC prions are tightly regulated. Lastly, other mammalian prion-like proteins described to date reside in post-mitotic or rarely dividing neurons or myocytes. Remarkably, the kinetics of MAVS and ASC prion propagation is sufficient to sustain the prion state in yeast cells that divide once every ninety minutes, and does so independently of the amyloid-severing factor Hsp104 that is required for the propagation of most other prions in yeast. This suggests that death domain prions possess a unique mechanism of fiber fragmentation. Despite these unusual features, $MAVS^{CARD}$ and $ASC^{PYD}$ exhibit the cardinal hallmarks of prions, including irreversible conversion to stable filamentous structures, cytoplasmic multigenerational inheritance (in yeast), and most importantly, an ability to template naïve molecules of the same protein into self-perpetuating conformations.

In sum, our data demonstrate that MAVS and ASC contain prion domains that allow these proteins to form self-perpetuating polymers, which are highly potent in activating and propagating immune and inflammatory responses. For both proteins, conversion to the active prion form is tightly regulated by upstream sensors of microbial or cellular danger signals.

Such tight regulation of nucleation followed by efficient polymerization produces a highly sensitive and robust digital response to harmful insults. It is likely that signal transduction through prion-like switches is also deployed in other biological pathways.


**Figure 26. Model for RIG-I MAVS signaling.**

The binding of 5'ppp-RNA releases RIG-I from its auto-inhibited state. RIG-I then binds to K63 polyubiquitin chains and form a tetrameric complex that interacts with MAVS on the mitochondria, bringing multiple MAVS proteins into proximity. This transient nucleation event between RIG-I$^{CARDs}$ and MAVS$^{CARD}$ converts MAVS$^{CARD}$ into its prion form, and allows further recruitment of other MAVS molecules into the prion-like fibers through CARD-CARD interactions. The large MAVS signalosome is then able to recruit downstream factors such as TRAF2, 5, and 6 to activate IRF3 to produce type-I interferons and other antiviral molecules.

# PART IV

# EXPERIMENTAL PROCEDURES

## Yeast Strains and Media

The generation of DD-Sup35C fusion strains was similar to that described for the generation of yeast prion domain (PrD)-Sup35C fusions (Alberti et al., 2009). First, a yeast strain RHY225, containing a chromosomal deletion of *SUP35* covered by a plasmid-borne version of *SUP35C*, was transformed with plasmids expressing DD-Sup35C fusions. Individual transformants were then plated onto 5-FOA to select against the pAG416-*ADH2*-Ure2-Sup35C covering plasmid. FOA resistant colonies were then plated onto YPE to ensure that they did not contain mitochondrial defects prior to being plated to YPD to assess Sup35C function. The resultant strains have the DD-Sup35C fusions as the only version of Sup35. Please see Supplemental Tables 1 and 2 for complete lists of primers and yeast strains used in the study.

Yeast transformations were performed using a standard lithium-acetate transformation protocol (Gietz et al., 1995). Standard yeast media and growth conditions were used. Media contained the following carbon sources: 2% dextrose (SD), 4% dextrose (¼YPD), 2% galactose (SG), or 2% ethanol (YPE). ¼YPD was used to enhance colony color discrimination, and was prepared as described (Parham et al., 2001). Where indicated, hygromycin B (HB) and nourseothricin (NAT) were used at a concentration of 500µg/ml and 100µg/ml, respectively.

## Yeast Prion Assays, Reconstitution, SDD-AGE

To test for prion activities in yeast, strains constitutively expressing the indicated DD-Sup35C fusions were transformed with inducing plasmids encoding DD-, RIG-I(N)-, $NLRP3^{PYD}$-, or $AIM2^{FL}$-EYFP fusions driven from a *GAL1* promoter. Selected individual colonies (usually in triplicates or quadruplicates) were then grown to confluence in SD-ura media, followed by washing 3 times in water to remove residual glucose. Cells were then resuspended in either SD-ura (no induction) or SG-ura (induction) for two days before being plated as indicated. After growth at 30°C for 2-3 days, ¼YPD plates were moved to 4°C overnight and then photographed the following day. SD-ade and SD-ura plates were photographed after 3-6 days of incubation at 30°C.

To reconstitute inflammasome signaling in yeast, strains constitutively expressing $ASC^{FL}$-Sup35C were transformed with the indicated inducing plasmid and a HPH- or NAT-marked plasmid constitutively expressing pro-caspase-1 from the *SUP35* promoter. Individual transformant colonies were grown under continuous selection for the caspase-1 plasmid and induced as described above, before being plated onto YPD+HB or YPD+NAT. White individual colonies arising on these plates were then re-streaked to identify single [$ASC^{FL}$+] (white) and [$asc^{fl}$-] (red) clones (arising through the frequent spontaneous loss of [$ASC^{FL}$+]), which were then photographed. Individual clones were then subjected to alkaline lysis followed by western blot analysis (Kushnirov, 2000). Briefly, clones were picked and incubated in 0.2M NaOH for 5 minutes in PCR strips. Following brief centrifugation, cell pellets were resuspended in 1x SDS-PAGE sample buffer and boiled at 95°C for 5 minutes. After spinning down the cell debris, a fraction of the supernatant was subjected to SDS-PAGE followed by caspase-1 immunoblotting.

SDD-AGE was carried out as described with minor modifications (Holmes et al., 2013). Briefly, yeast were grown to equal density in 1ml YPD in 96 well blocks (Nunc P8241) followed by centrifugation at 3000g. After washing with water, cells were centrifuged again and mixed with 100ul of acid-washed glass beads along with 70µl of Buffer A (100mM Tris-HCl pH8.0, 2mM $MgCl_2$, 3x HALT protease inhibitor cocktail, and 25U/ml Benzonase). Blocks were then shaken at max speed for 5 minutes, rotated, then shaken again for 5 minutes, on a QIAGEN tissuelyzer. After brief centrifugation, 30µl of 4X sample buffer (2x TAE, 20% glycerol, 8% SDS, 0.05% bromophenol blue) was added to each sample. The block was briefly vortexed at max speed followed by centrifugation at 3000g to spin down the cell debris. After incubation at room temperature for 5 minutes, the samples were loaded onto a horizontal 1.5% agarose gel in 0.5x TAE and 0.1% SDS. After electrophoresis at 50V for 3 hours, the agarose gel was transferred to a Hybond ECL nitrocellulose membrane and subjected to standard western blotting with specific antibodies. For SDS-PAGE western analysis of DD-Sup35C expression, 2.5% β-mercaptoethanol was added to fractions of the same lysates, followed by incubation at 95°C for 5 minutes before loading onto a 15% SDS-PAGE gel.

**Recombinant $ASC^{PYD}$ Purification**

The bacterial expression vector pET-28a-$His_6$-Sumo-$ASC^{PYD}$ was transformed into BL-21(pLys). Protein expression was induced with 0.2 mM IPTG at 18°C overnight. Cells were lysed using a French press in a Buffer B [20mM Tris-HCl pH 8.0, 500mM NaCl, 5 mM β-mercaptoethanol, 20 mM imidazole, 0.5mM PMSF, and 1x EDTA free complete protease

inhibitor cocktail(Roche)] followed by centrifugation at 12,000g for 20 minutes at 4°C. $His_6$-Sumo-$ASC^{PYD}$ was purified from the supernatant using Ni-NTA beads using a step elution (50-250mM imidazole). The Sumo tag was cleaved during overnight dialysis in Buffer C (20mM Tris-HCl pH 8.0, 150 mM NaCl, 5 mM β-mercaptoethanol) with a 500:1 mass ratio of Sumo-$ASC^{PYD}$:Sumo protease. The dialysed sample was centrifuged at 20,000g and the supernatant filtered (0.45μm) and loaded onto a 24-mL Superdex-200 gel filtration column equilibrated with Buffer D (20mM Tris-HCl pH8.0, 120mM NaCl, 1mM DTT, and 0.02% CHAPS). $ASC^{PYD}$ concentration in the void volume fraction was estimated by comparing to BSA standards using Coomassie blue staining and subjected to EM analysis.

### *In vitro* ASC Activity Assay

293T cells transfected with indicated pcDNA3-ASC WT or mutant plasmids were lysed in buffer E [10mM Tris-HCl pH 7.5, 10mM KCl, 1.5mM $MgCl_2$, 1x EDTA free complete protease inhibitor cocktail (Roche)] and centrifuged at 20,000g (S20) for 15 minutes. ~50μg of the supernatant was mixed with 20μg of lysate from 293T cells stably expressing pro-caspase1 and pro-IL-1β in buffer E and incubated at 30°C for the indicated time. Indicated amounts of $ASC^{PYD}$ or NM fibers were incubated with ~50μg of lysate (S20) from 293T cells stably expressing $ASC^{FL}$-GFP and 20μg of S20 from 293T cells stably expressing pro-caspase-1 in buffer E in a final volume of 11μl at 30°C for 60 minutes. Western blotting for p10 was done using a 15% PAGE gel.

### Inflammasome Reconstitution Assay in Cells

Approximately 18 hours after transfection of 200ng of ASC WT or mutant into 293T cells stably expressing flag-NLRP3, pro-caspase-1, and pro-IL-1β-flag in a 12-well plate, 10μM Nigericin was added to culture media for 45 or 90 minutes. The culture supernatant was concentrated using a 5kD filter followed by SDS-PAGE analysis. Cells were lysed in buffer F (50mM Tris HCl pH 8.0, 100mM NaCl, 10% glycerol, 0.5% NP40, and 1x protease inhibitor cocktail) followed by centrifugation at 500g. The supernatant was subjected to SDS-PAGE and immunoblotting analysis.

**Sup35$^{NM}$ Assays in the Mammalian System**

NM fibers were generated essentially as described (Alberti et al., 2009). Briefly, pAED4-NM-$His_7$ (from Susan Lindquist) was transformed into BL21(pLys) followed by induction with 1mM IPTG at 30°C for 3 hours. Cells were lysed in buffer G (6M Guanidine-HCl, 20mM Tris-HCl 8.0, 5mM β-mercaptoethanol) followed by centrifugation at 12,000g. The supernatant was incubated with Ni-NTA beads and eluted in buffer H (100mM acetate pH 4.0, 8M urea, 5mM β-mercaptoethanol). Following methanol precipitation (~5:1 ratio of methanol:eluate volume) and incubation at -80°C overnight, the eluate was centrifuged at 12,000g and the pellet resuspended in buffer I (6M Guanidine-HCl, 100mM potassium phosphate pH 7), boiled at 95°C, followed by rapid dilution by PBS to 10μM final fiber concentration and subjected to overnight rotation at 60 RPM (4°C).

A final concentration of 1μM NM fibers was added to culture media of 293T cells expressing NM-ASC$^{CARD}$ or NM-ASC$^{PYD}$ or to culture media of *IFNβ*-Luc 293T cells

expressing NM or NM-MAVS as indicated in the legends. Twenty-four hours later, the cell lysates were subjected to caspase-1 western or luciferase assay as indicated. Mitochondria fraction (P5) from one confluent 10-cm dish of 293T cells stably expressing NM-MAVS was resuspended in 20μl buffer E and incubated with 500ng NM fibers (NM fiber-P5 mix) at RT for 30 minutes. Then, 2ul of the NM fiber-P5 mix was incubated with ~40μg of 293T S20, Mg-ATP buffer, and $^{35}$S-IRF3 at 30°C for 1 hour as described previously for the *in vitro* IRF3 assay (Liu et al., 2013; Zeng et al., 2009). Fifty microliter of S1 (supernatant after 1000g centrifugation) from 293T cells transiently transfected with NM-ASC$^{CARD}$ or NM-ASC$^{PYD}$ was incubated with 500ng NM fiber at RT for 30 minutes. Six microliter of the mix was then incubated with lysate from 293T cells stably expressing pro-caspase-1 at 30°C for one hour for caspase-1 activity assay as described above.

**Plasmids, Cell Lines, and Antibodies**

AIM2, NLRP3, ASC, pro-caspase-1, IL1β, and NLRC4 constructs were of mouse origin. RIG-I and MAVS constructs were of human origin. RIG-I(N) (N200), MAVS$^{CARD}$(N100), AIM2$^{FL}$, NLRP3$^{PYD}$(N100), ASC$^{PYD}$(N90), ASC$^{CARD}$(C90), ASC$^{FL}$, pro-caspase-1, NM, NLRC4$^{N100}$, and capase-1 C284A were cloned into pDONR221 using two step PCR (Alberti et al., 2009). The resulting entry clones were then recombined into pAG426-*GAL*-ccdb-EYFP [RIG-I(N), MAVS$^{CARD}$, AIM2$^{FL}$, NLRP3$^{PYD}$, ASC$^{PYD}$, and NM] or into pAG416-*TEF2*-ccdb-Sup35C (MAVS$^{CARD}$, WT and mutant ASC$^{PYD}$, and ASC$^{FL}$). Entry clones for RIG-I(N), ASC$^{CARD}$, and mutant and WT MAVS$^{CARD}$, were recombined into pAG416-*ADH1*-ccdb-Sup35C. All other DD-Sup35C fusion candidates used in the

screen were generated in the same way as $ASC^{CARD}$ using primers listed in Table 2. Pro-caspase-1 was cloned into pAG41HPH-*SUP35*-ccdb or pAG41NAT-*SUP35*-ccdb harboring respective HB- or NAT-resistance cassettes. For mammalian expression, NM, NM-MAVS (NM-MAVSΔN77), NM-$ASC^{PYD}$, NM-$ASC^{CARD}$, ASC WT and mutants, HA-ASC, and HA-HET-$s^{PrD}$-$ASC^{\Delta PYD}$ were cloned into pcDNA3 and all, except for NM-MAVS, have C-terminal FLAG tags.

For the generation of cell lines stably expressing indicated inflammasome components or NM-MAVS, lentiviral expression constructs pTY-*EF1α*-zeocinR-2a-pro-caspase-1, pTY-*EF1α*-puroR-2a-pro-IL-1β-Flag, pTY-*EF1α*-Flag-NLRP3-IRES-HygroR, pTY-*EF1α*-$ASC^{FL}$-GFP-IRES-HygroR, pTY-*EF1α*-puroR-2a-NM-MAVS, pTY-*EF1α*-$NWD2^{N30}$-$NLRP3^{\Delta PYD}$-Flag-HygroR, pTY-*EF1α*-NLRP3-Flag-HygroR vectors were used to make lentiviruses for subsequent infection of 293T cells. Please see (Liu et al., 2013; Tanaka and Chen, 2012) for a detailed description of lentiviral construction. 293T *IFNβ*-Luc reporter cells were described previously (Chiu et al., 2009).

Antibodies to MAVS (SC-166583, Santa Cruz Biotechnology), Flag M2 (Sigma), $ASC^{PYD}$ (AL177, Adipogen), NLRP3 (Cryo-2, Adipogen), Caspase-1 (SC-514, Santa Cruz Biotechnology), IL-1β (AB-401-NA, R&D systems), and GFP (A11122, Invitrogen) were used according to manufacturer's recommendation. Antibody to Sup35C (clone UIC-M 11/12, 4C10 BE4) was purchased through Cocalico Biologicals with permission from Susan Liebman.

**Cytoduction**

Recipient strains (ZJC1338c, ZJC217c) used for cytoduction were generated from strain L2958, generously provided by Sue Liebman. Briefly, Ade+ or ade- donor strains were mated with ade- recipient strains on YPD for 12 hours. A mutant *kar1* (*kar1-15*) in the recipient strain prevented nuclear fusion. Furthermore, in addition to a recessive cycloheximide resistance mutation, the recipient also contains mitochondrial DNA defect that prevents growth on plates containing non-fermentable carbon such as ethanol (YPE). Cytoductants containing donor cytoplasm and recipient nucleus were selected on ethanol containing plate supplemented with 3 mg/liter cyclohexamide (YPE+CHX). YPE+CHX selects against the donor and diploids as they cannot grow in the presence of CHX. Individual cytoductants on YPE+CHX were resuspended in water and plated onto ¼YPD and SD-ade as indicated.

**Yeast Mating**

The indicated MATa (leu+) and MATα (trp+) strains were mated on YPD plates for 12 hours followed by plating to SD-leu-trp plates. Single diploid clones were then passaged onto SD-trp plates to allow for the loss of the leu+ DD-Sup35C plasmid. The SD-trp plates were then replicated to SD-leu plates to select for clones that have lost the leu+ DD-Sup35C plasmid (i.e. colony from SD-trp did not grow on SD-leu when replicated). Individual leu- diploid clones were resuspended in water and plated onto SD-ade and ¼YPD.

**Sucrose Gradient Ultracentrifugation**

Sucrose gradient ultracentrifugation was performed as described previously (Hou et al., 2011). One confluent 15-cm dish of 293T cells stably expressing Flag-NLRP3 and $ASC^{FL}$-GFP was treated with 10μM Nigericin (Sigma) for 60 minutes and lysed in buffer E followed by centrifugation at 1000g to remove cell debris. Supernatant was loaded onto a 20-60% sucrose cushion and centrifuged at 170,000g using a swing bucket rotor for 2 hours at 4°C. Aliquots of individual fractions were subjected to western blot analysis for $ASC^{FL}$-GFP and activity assay by incubation with 20μg of lysate (S20) from 293T cells stably expressing pro-caspase-1 in buffer E at 30°C for one hour. For *in vitro* $ASC^{FL}$-GFP activation, ~4mg of 293T+$ASC^{FL}$-GFP S20 was incubated with or without 50ng of $ASC^{PYD}$ fibers at 30°C for 30 minutes followed by sucrose gradient analysis and *in vitro* caspase-1 assay as described above.

**Cell Culture**

All transfections were done with Lipofectamine 2000 (Invitrogen) unless stated otherwise. 293T cells were maintained in DMEM supplemented with 10% calf serum and 1x penicillin and streptomycin. In cases where culture media were to be collected for western analysis, treatments (i.e. NM fiber, Nigericin) were done in OPTI-MEM reduced serum media (Invitrogen).

**Confocal Microscopy**

Images were taken using a Zeiss LSM510 confocal microscope at a magnification of 63x.

**Electron Microscopy**

Copper grids (Ted Pella Inc., Redding, CA) coated with a layer of thin carbon film (3-5 nm) were rendered hydrophilic by negative glow-discharge in air. 2.5 □l purified ASC sample was loaded onto the grids. After 30 s of incubation on the grid at room temperature, the sample was stained with 2.0% phosphotungstic acid (PTA) at pH 8.0 and blotted dry. Samples were imaged using a JEOL 2200FS FEG electron microscope operating at 200 kV at a nominal magnification of 25,000× (1.54 Å/pixel at the detector level) using a defocus range of −0.7 to −1.5 μm. Images were recorded with an electron dose of ~20$e^-$/Å$^2$ on a 4K x 4K K2 Summit Direct Detector (Gatan, Inc.) using electron-counting mode.

**Table 2. Yeast strains used and described in this study.**

| Name | Relevant Genotypes | Source |
|---|---|---|
| YJW508 | MATa, leu2-3,112; his3-11,15; trp1-1; ura3-1; ade1-14; can1-100; [PSI+]; [PIN+]; | (Osherovich et al., 2004) |
| YJW584 | MATa, leu2-3,112; his3-11,15; trp1-1; ura3-1; ade1-14; can1-100; [psi-]; [PIN+]; | (Osherovich et al., 2004) |
| RHY225 | MATa, leu2-3,112; his3-11,15; trp1-1; ura3-1; ade1-14; can1-100; [PIN+]; sup35::KanMX4; pAG416ADH-Ure2-Sup35C | (Alberti et al., 2009) |
| RHY1271b | MATa, leu2-3,112; his3-11,15; trp1-1; ura3-1; ade1-14; can1-100; [PIN+]; sup35::KanMX4; pAG415TEF-MAVS-CARD-Sup35C; [mavs$^{card}$-] | This study |
| RHY1312 | MATa, leu2-3,112; his3-11,15; trp1-1; ura3-1; ade1-14; can1-100; [PIN+]; sup35::KanMX4; pAG415TEF-MAVS-CARD-Sup35C; [MAVS$^{CARD}$+] | This study |
| RHY1338 | MATα, leu2-3,112; his3-11,15; trp1-1; ura3-1; ade1-14; can1-100; [PIN+]; sup35::KanMX4; pAG414TEF-MAVS-CARD-Sup35C; [mavs$^{card}$-] | This study |
| ZJC10 | MATa, leu2-3,112; his3-11,15; trp1-1; ura3-1; ade1-14; can1-100; [PIN+]; sup35::KanMX4; pAG415ADH-RIG-I(N)-Sup35C | This study |
| ZJC172 | MATa, leu2-3,112; his3-11,15; trp1-1; ura3-1; ade1-14; can1-100; [PIN+]; sup35::KanMX4; pAG415ADH-MAVS-CARD(WT)-Sup35C; [mavs$^{card}$-] | This study |
| ZJC173 | MATa, leu2-3,112; his3-11,15; trp1-1; ura3-1; ade1-14; can1-100; [PIN+]; sup35::KanMX4; pAG415ADH-MAVS-CARD(E26A)-Sup35C; [mavs$^{card}$-] | This study |
| ZJC175 | MATa, leu2-3,112; his3-11,15; trp1-1; ura3-1; ade1-14; can1-100; [PIN+]; sup35::KanMX4; pAG415ADH-MAVS-CARD(R64A)-Sup35C; [mavs$^{card}$-] | This study |
| ZJC176 | MATa, leu2-3,112; his3-11,15; trp1-1; ura3-1; ade1-14; can1-100; [PIN+]; sup35::KanMX4; pAG415ADH-MAVS-CARD(R65A)-Sup35C; [mavs$^{card}$-] | This study |
| ZJC172a | MATa, leu2-3,112; his3-11,15; trp1-1; ura3-1; ade1-14; can1-100; [PIN+]; sup35::KanMX4; pAG415ADH-MAVS-CARD(WT)-Sup35C; [MAVS$^{CARD}$+] | This study |
| ZJC92 | MATa, leu2-3,112; his3-11,15; trp1-1; ura3-1; ade1-14; can1-100; [PIN+]; | This study |

| | | |
|---|---|---|
| | sup35::KanMX4; pAG415ADH-APAF1-CARD-Sup35C | |
| ZJC93 | MATa, leu2-3,112; his3-11,15; trp1-1; ura3-1; ade1-14; can1-100; [PIN+]; sup35::KanMX4; pAG415ADH-ASC-CARD-Sup35C | This study |
| ZJC94 | MATa, leu2-3,112; his3-11,15; trp1-1; ura3-1; ade1-14; can1-100; [PIN+]; sup35::KanMX4; pAG415ADH-ASC-PYD-Sup35C | This study |
| ZJC95 | MATa, leu2-3,112; his3-11,15; trp1-1; ura3-1; ade1-14; can1-100; [PIN+]; sup35::KanMX4; pAG415ADH-BCL10-CARD-Sup35C | This study |
| ZJC96 | MATa, leu2-3,112; his3-11,15; trp1-1; ura3-1; ade1-14; can1-100; [PIN+]; sup35::KanMX4; pAG415ADH-CARMA1-CARD-Sup35C | This study |
| ZJC97 | MATa, leu2-3,112; his3-11,15; trp1-1; ura3-1; ade1-14; can1-100; [PIN+]; sup35::KanMX4; pAG415ADH-CASP8-DEDs-Sup35C | This study |
| ZJC98 | MATa, leu2-3,112; his3-11,15; trp1-1; ura3-1; ade1-14; can1-100; [PIN+]; sup35::KanMX4; pAG415ADH-CASP9-CARD-Sup35C | This study |
| ZJC99 | MATa, leu2-3,112; his3-11,15; trp1-1; ura3-1; ade1-14; can1-100; [PIN+]; sup35::KanMX4; pAG415ADH-FADD-DD-Sup35C | This study |
| ZJC100 | MATa, leu2-3,112; his3-11,15; trp1-1; ura3-1; ade1-14; can1-100; [PIN+]; sup35::KanMX4; pAG415ADH-FADD-DED-Sup35C | This study |
| ZJC101 | MATa, leu2-3,112; his3-11,15; trp1-1; ura3-1; ade1-14; can1-100; [PIN+]; sup35::KanMX4; pAG415ADH-FAS-DD-Sup35C | This study |
| ZJC102 | MATa, leu2-3,112; his3-11,15; trp1-1; ura3-1; ade1-14; can1-100; [PIN+]; sup35::KanMX4; pAG415ADH-MALT1-DD-Sup35C | This study |
| ZJC103 | MATa, leu2-3,112; his3-11,15; trp1-1; ura3-1; ade1-14; can1-100; [PIN+]; sup35::KanMX4; pAG415ADH-MYD88-DD-Sup35C | This study |
| ZJC105 | MATa, leu2-3,112; his3-11,15; trp1-1; ura3-1; ade1-14; can1-100; [PIN+]; sup35::KanMX4; pAG415ADH-NLRP3-PYD-Sup35C | This study |
| ZJC106 | MATa, leu2-3,112; his3-11,15; trp1-1; ura3-1; ade1-14; can1-100; [PIN+]; sup35::KanMX4; pAG415ADH-NOD1-CARD-Sup35C | This study |
| ZJC107 | MATa, leu2-3,112; his3-11,15; trp1-1; ura3-1; ade1-14; can1-100; [PIN+]; sup35::KanMX4; pAG415ADH-NOD2-CARDs-Sup35C | This study |
| ZJC108 | MATa, leu2-3,112; his3-11,15; trp1-1; ura3-1; ade1-14; can1-100; [PIN+]; sup35::KanMX4; pAG415ADH-RIP1-DD-Sup35C | This study |
| ZJC109 | MATa, leu2-3,112; his3-11,15; trp1-1; ura3-1; ade1-14; can1-100; [PIN+]; sup35::KanMX4; pAG415ADH-RIP2-CARD-Sup35C | This study |
| ZJC110 | MATa, leu2-3,112; his3-11,15; trp1-1; ura3-1; ade1-14; can1-100; [PIN+]; sup35::KanMX4; pAG415ADH-TRADD-DD-Sup35C | This study |
| ZJC151 | MATa, leu2-3,112; his3-11,15; trp1-1; ura3-1; ade1-14; can1-100; [PIN+]; sup35::KanMX4; pAG415TEF-ASC-PYD-Sup35C; [$asc^{pyd}$-] | This study |
| ZJC217 | MATα, leu2-3,112; his3-11,15; trp1-1; ura3-1; ade1-14; can1-100; [PIN+]; sup35::KanMX4; pAG414TEF-ASC-PYD-Sup35C; [$asc^{pyd}$-] | This study |
| ZJC264 | MATa, leu2-3,112; his3-11,15; trp1-1; ura3-1; ade1-14; can1-100; [PIN+]; sup35::KanMX4; pAG415TEF-ASC-PYD(R41A)-Sup35C; [$asc^{pyd}$-] | This study |
| ZJC265 | MATa, leu2-3,112; his3-11,15; trp1-1; ura3-1; ade1-14; can1-100; [PIN+]; sup35::KanMX4; pAG415TEF-ASC-PYD(D48A)-Sup35C; [$asc^{pyd}$-] | This study |
| ZJC267 | MATa, leu2-3,112; his3-11,15; trp1-1; ura3-1; ade1-14; can1-100; [PIN+]; sup35::KanMX4; pAG415TEF-ASC-PYD(G40A)-Sup35C; [$asc^{pyd}$-] | This study |
| ZJC270 | MATa, leu2-3,112; his3-11,15; trp1-1; ura3-1; ade1-14; can1-100; [PIN+]; sup35::KanMX4; pAG415TEF-ASC-FL-Sup35C; [$asc^{fl}$-] | This study |
| ZJC1338a | MATa/α, leu2-3,112/leu2-3,112; his3-11,15/his3-11,15; trp1-1/ trp1-1; ura3-1/ura3-1; ade1-14/ade1-14; can1-100/can1-100; [PIN+]; sup35/sup35::KanMX4; pAG414TEF-MAVS-CARD-Sup35C; [$mavs^{card}$-] | This study |
| ZJC1338b | MATa/α, leu2-3,112/leu2-3,112; his3-11,15/his3-11,15; trp1-1/ trp1-1; ura3-1/ura3-1; ade1-14/ade1-14; can1-100/can1-100; [PIN+]; sup35/sup35::KanMX4; pAG414TEF- | This study |

| | | |
|---|---|---|
| | MAVS-CARD-Sup35C; [$MAVS^{CARD}$+] | |
| ZJC217a | MATa/α, leu2-3,112/leu2-3,112; his3-11,15/his3-11,15; trp1-1/ trp1-1; ura3-1/ura3-1; ade1-14/ade1-14; can1-100/can1-100; [PIN+]; sup35/sup35::KanMX4; pAG414TEF-ASC-PYD-Sup35C; [$asc^{pyd}$-] | This study |
| ZJC217b | MATa/α, leu2-3,112/leu2-3,112; his3-11,15/his3-11,15; trp1-1/ trp1-1; ura3-1/ura3-1; ade1-14/ade1-14; can1-100/can1-100; [PIN+]; sup35/sup35::KanMX4; pAG414TEF-ASC-PYD-Sup35C; [$ASC^{PYD}$+] | This study |
| ZJC151a | MATa, leu2-3,112; his3-11,15; trp1-1; ura3-1; ade1-14; can1-100; [PIN+]; sup35::KanMX4; pAG415TEF-ASC-PYD-Sup35C; [$ASC^{PYD}$+] | This study |
| ZJC217c | MATα, ade1-14, leu2-3,112, his3-Δ200, trp1-289, ura3-52,sup35::KanMX4; pAG414TEF-ASC-PYD-Sup35C; kar1 cyhR | This study |
| ZJC1338c | MATα, ade1-14, leu2-3,112, his3-Δ200, trp1-289, ura3-52,sup35::KanMX4; pAG414TEF-MAVS-CARD-Sup35C; kar1 cyhR | This study |
| ZJC270a | MATa, leu2-3,112; his3-11,15; trp1-1; ura3-1; ade1-14; can1-100; [PIN+]; sup35::KanMX4; pAG415TEF-ASC-FL-Sup35C; [$ASC^{FL}$+] | This study |
| ZJC270b | MATa, leu2-3,112; his3-11,15; trp1-1; ura3-1; ade1-14; can1-100; [PIN+]; sup35::KanMX4; pAG415TEF-ASC-FL-Sup35C; pAG41HPH-Sup35-pro-caspase-1; [$asc^{fl}$-] | This study |
| ZJC270c | MATa, leu2-3,112; his3-11,15; trp1-1; ura3-1; ade1-14; can1-100; [PIN+]; sup35::KanMX4; pAG415TEF-ASC-FL-Sup35C; pAG41HPH-Sup35-pro-caspase-1; [$ASC^{FL}$+] | This study |
| ZJC270d | MATa, leu2-3,112; his3-11,15; trp1-1; ura3-1; ade1-14; can1-100; [PIN+]; sup35::KanMX4; pAG415TEF-ASC-FL-Sup35C; pAG41NAT-Sup35-pro-caspase-1; [$asc^{fl}$-] | This study |
| ZJC270e | MATa, leu2-3,112; his3-11,15; trp1-1; ura3-1; ade1-14; can1-100; [PIN+]; sup35::KanMX4; pAG415TEF-ASC-FL-Sup35C; pAG41NAT-Sup35-pro-caspase-1; [$ASC^{FL}$+] | This study |

All strains are derivatives of YJW508 (Osherovich et al. 2004).

**Table 3. Primers used for cloning candidate DDs.**

| DD Domain | Primer |
|---|---|
| APAF1 CARD For | aggagataacaaaatgGATGCAAAAGCTCGAAATTG |
| APAF1 CARD Rev | caagaaagctgggtcTTTACCACTGGAAGAAGAGAC |
| ASC CARD For | aggagataacaaaatgAGTACAGCCAGAACAGGACAC |
| ASC CARD Rev | caagaaagctgggtcGCTCTGCTCCAGGTCCATCACCAAGTAGG |
| ASC PYR For | aggagataacaaaatgGGGCGGGCACGAGATG |
| ASC PYR Rev | caagaaagctgggtcCTCTTTAGTCGTTTGCAGCTG |
| BCL10 CARD For | aggagataacaaaatgGAGCCCACCGCACCGTC |
| BCL10 CARD Rev | caagaaagctgggtcAAGTTTGAGCACTTCATCTGTAATCTTCTG |
| CARMA1 CARD For | aggagataacaaaatgTACATGGAGACGCTGAAGG |
| CARMA1 CARD Rev | caagaaagctgggtcCTCTTTTCCTGTCACCAGTTTGTACAGTTCTG |
| CASP8 DED For | aggagataacaaaatgGACTTCAGCAGAAATCTTTATG |
| CASP8 DED Rev | caagaaagctgggtcGAATTCTTCATAGTCGTTG |
| CASP9 CARD For | aggagataacaaaatgGACGAAGCGGATCGGC |
| CASP9 CARD Rev | caagaaagctgggtcCTTCGACAACTTTGCTGC |
| FADD DD For | aggagataacaaaatgGCGCCTGGGGAAGAAGAC |
| FADD DD Rev | caagaaagctgggtcACTCCTGTTCTGGAGGTCACGG |
| FADD DED For | aggagataacaaaatgACCGAGCTCAAGTTCC |
| FADD DED Rev | caagaaagctgggtcCAGGGAGGCGAGCAGCTC |
| FAS DD For | aggagataacaaaatgGCAATAAATTTATCTGATG |
| FAS DD Rev | caagaaagctgggtcGACCAAGGATTGGATTTCATTTCTGAAGTTTG |
| MALT1 DD For | aggagataacaaaatgCCACTGCTGCGGAGGCTCAG |
| MALT1 DD Rev | caagaaagctgggtcTGACTCTGGGTTTACAG |
| MYD88 DD For | aggagataacaaaatgGCGGGGTCTGCGGC |
| MYD88 DD Rev | caagaaagctgggtcCTTCAAGATATACTTTTG |
| NLRP3 PYR For | aggagataacaaaatgACGAGTGTCCGTTGCAAGC |
| NLRP3 PYR Rev | caagaaagctgggtcGGAATGTGATGTACACGTGTC |
| NOD1 CARD For | aggagataacaaaatgGAAGAGCAGGGCCACAGTG |
| NOD1 CARD Rev | caagaaagctgggtcAGAGAAGCCGATCTCCAG |
| RIP1 DD For | aggagataacaaaatgTTTGATAATACCACTAGTC |
| RIP1 DD Rev | caagaaagctgggtcGTTCTGGCTGACGTAAATC |
| RIP2 CARD For | aggagataacaaaatgCTGCAGCCTGGTATAGC |
| RIP2 CARD Rev | caagaaagctgggtcTGGTGATCTAGAAACC |
| TRADD DD For | aggagataacaaaatgAATCGGCCGCTGAGC |
| TRADD DD Rev | caagaaagctgggtaAGCGAGGCCGCCATTGGGATCG |
| NOD2 CARD For | aggagataacaaaatgTTTCAGGCACAGAGGAGC |
| NOD2 CARD Rev | caagaaagctgggtcCTGAACATGTTGTAGAAGG |
| | |
| *Universal For | GGGGACAAGTTTGTACAAAAAAGCAGGCTTCGAAGGAGATAACAAAATG |
| *Universal Rev | GGGGACCACTTTGTACAAGAAAGCTGGGTC |

*Primers used for the second PCR to generate DD entry clones for Gateway® cloning.

**Table 4. Other relevant primers for PCR and cloning**

| Primer Name | Sequence |
|---|---|
| HA-ASC For | TTTggatccATGTACCCcTACGATGTTCCTGATTACGCTgggcgggcacg |
| ASC Rev | tttttGAATTCtcagctctgctccaggtccatcac |
| HA-HETs PrD For | TTTggatccATGTACCCATACGATGTTCCAGATTACGCTaAAATAGATGC |
| HETs PrD-ASCΔPYD Sense | GGAAGGGATTTTGGGACAATgagtctggagctgtggcag |
| HETs PrD-ASCΔPYD Antisense | ctgccacagctccagactcATTGTCCCAAAATCCCTTCC |
| NWD2 For | aaaaGCGGCCGCatggcaaatcaggttcg |
| NWD2 N30-NLRP3ΔPYD Sense | gctcgagcgacttcctcccgTCTATGGTATGCCAGGAG |
| NWD2 N30-NLRP3ΔPYD Antisense | CTCCTGGCATACCATAGAcgggaggaagtcgctcgagc |
| NLRP3-Flag Rev | TTTTgctagcTCACTTGTCATCATCATCTTTGTAGTCccaggaaatctcg |
| NWD2 N30-Flag Rev | TTTTgctagcTCACTTGTCATCATCATCTTTGTAGTCcgggaggaagtcg |
| NWD2 N50-Flag Rev | TTTTgctagcTCACTTGTCATCATCATCTTTGTAGTCgcggtggcatcgggc |
| NLRP3 For | ttttGCGGCCGCatgacgagtgtccgttg |
| NM For | TTTTggatccATGTCGGATTCAAACCAAGG |
| NM-MAVSΔCARD Sense | GAAGAAGTGGATGACGAAGTTGTTAACGATGGCTGTGAGCTAGTTGATCT CGCGGACGAAG |
| NM-MAVSΔCARD Antisense | CTTCGTCCGCGAGATCAACTAGCTCACAGCCATCGTTAACAACTTCGTCAT CCACTTCTTC |
| MAVS Rev | GCAGTActcgagCTAGTGCAGACGCCGCCGGTACAGCACCAC |
| NM-Flag Rev | TCGACTacgcgtCTACTTGTCATCGTCGTCCTTGTAGTCATCGTTAACAACTTC GTCATCC |
| NM-ASC CARD Sense | GTGGATGACGAAGTTGTTAACGATAGTACAGCCAGAACAGGACACTTTG |
| NM-ASC CARD Antisense | CAAAGTGTCCTGTTCTGGCTGTACTATCGTTAACAACTTCGTCATCCAC |
| ASC CARD-Flag Rev | aaaagaattcTCACTTGTCATCATCATCCTTGTAGTCGCTCTGCTCCAGG |
| NM-ASC PYD Sense | GAAGTGGATGACGAAGTTGTTAACGATATGGGGCGGGCACGAGATGC |
| NM-ASC PYD Antisense | GCATCTCGTGCCCGCCCCATATCGTTAACAACTTCGTCATCCACTTC |
| ASC PYD-Flag Rev | aaaagaattcTCACTTGTCATCATCATCCTTGTAGTCTTCTTTAGTCGTT |

## PART V

## REFERENCES

Agostini, L., Martinon, F., Burns, K., McDermott, M.F., Hawkins, P.N., and Tschopp, J. (2004). NALP3 forms an IL-1beta-processing inflammasome with increased activity in Muckle-Wells autoinflammatory disorder. Immunity *20*, 319-325.

Alberti, S., Halfmann, R., King, O., Kapila, A., and Lindquist, S. (2009). A systematic survey identifies prions and illuminates sequence features of prionogenic proteins. Cell *137*, 146-158.

Alberti, S., Halfmann, R., and Lindquist, S. (2010). Biochemical, cell biological, and genetic assays to analyze amyloid and prion aggregation in yeast. Methods Enzymol *470*, 709-734.

Atianand, M.K., Rathinam, V.A., and Fitzgerald, K.A. (2013). SnapShot: inflammasomes. Cell *153*, 272-272 e271.

Baltimore, D. (1995). Discovery of the reverse transcriptase. FASEB journal : official publication of the Federation of American Societies for Experimental Biology *9*, 1660-1663.

Belgnaoui, S.M., Paz, S., and Hiscott, J. (2011). Orchestrating the interferon antiviral response through the mitochondrial antiviral signaling (MAVS) adapter. Curr Opin Immunol.

Broz, P., Newton, K., Lamkanfi, M., Mariathasan, S., Dixit, V.M., and Monack, D.M. (2010). Redundant roles for inflammasome receptors NLRP3 and NLRC4 in host defense against Salmonella. J Exp Med *207*, 1745-1755.

Cai, X., Chen, J., Xu, H., Liu, S., Jiang, Q.X., Halfmann, R., and Chen, Z.J. (2014). Prion-like polymerization underlies signal transduction in antiviral immune defense and inflammasome activation. Cell *156*, 1207-1222.

Chernoff, Y.O., Lindquist, S.L., Ono, B., Inge-Vechtomov, S.G., and Liebman, S.W. (1995). Role of the chaperone protein Hsp104 in propagation of the yeast prion-like factor [psi+]. Science *268*, 880-884.

Chiu, Y.H., Macmillan, J.B., and Chen, Z.J. (2009). RNA polymerase III detects cytosolic DNA and induces type I interferons through the RIG-I pathway. Cell *138*, 576-591.

Collins, S.R., Douglass, A., Vale, R.D., and Weissman, J.S. (2004). Mechanism of prion propagation: amyloid growth occurs by monomer addition. PLoS Biol *2*, e321.

Daskalov, A., Paoletti, M., Ness, F., and Saupe, S.J. (2012). Genomic clustering and homology between HET-S and the NWD2 STAND protein in various fungal genomes. PLoS One *7*, e34854.

Fernandes-Alnemri, T., Wu, J., Yu, J.W., Datta, P., Miller, B., Jankowski, W., Rosenberg, S., Zhang, J., and Alnemri, E.S. (2007). The pyroptosome: a supramolecular assembly of ASC dimers mediating inflammatory cell death via caspase-1 activation. Cell Death Differ *14*, 1590-1604.

Fernandes-Alnemri, T., Yu, J.W., Datta, P., Wu, J., and Alnemri, E.S. (2009). AIM2 activates the inflammasome and cell death in response to cytoplasmic DNA. Nature *458*, 509-513.

Ferrao, R., and Wu, H. (2012). Helical assembly in the death domain (DD) superfamily. Curr Opin Struct Biol *22*, 241-247.

Gao, P., Ascano, M., Wu, Y., Barchet, W., Gaffney, B.L., Zillinger, T., Serganov, A.A., Liu, Y., Jones, R.A., Hartmann, G.*, et al.* (2013). Cyclic [G(2',5')pA(3',5')p] is the metazoan second messenger produced by DNA-activated cyclic GMP-AMP synthase. Cell *153*, 1094-1107.

Gietz, R.D., Schiestl, R.H., Willems, A.R., and Woods, R.A. (1995). Studies on the transformation of intact yeast cells by the LiAc/SS-DNA/PEG procedure. Yeast *11*, 355-360.

Halfmann, R., Jarosz, D.F., Jones, S.K., Chang, A., Lancaster, A.K., and Lindquist, S. (2012). Prions are a common mechanism for phenotypic inheritance in wild yeasts. Nature *482*, 363-368.

Halfmann, R., and Lindquist, S. (2008). Screening for amyloid aggregation by Semi-Denaturing Detergent-Agarose Gel Electrophoresis. J Vis Exp.

Halfmann, R., and Lindquist, S. (2010). Epigenetics in the extreme: prions and the inheritance of environmentally acquired traits. Science *330*, 629-632.

Holmes, D.L., Lancaster, A.K., Lindquist, S., and Halfmann, R. (2013). Heritable remodeling of yeast multicellularity by an environmentally responsive prion. Cell *153*, 153-165.

Hornung, V., Ablasser, A., Charrel-Dennis, M., Bauernfeind, F., Horvath, G., Caffrey, D.R., Latz, E., and Fitzgerald, K.A. (2009). AIM2 recognizes cytosolic dsDNA and forms a caspase-1-activating inflammasome with ASC. Nature *458*, 514-518.

Horvath, P., and Barrangou, R. (2010). CRISPR/Cas, the immune system of bacteria and archaea. Science *327*, 167-170.

Hou, F., Sun, L., Zheng, H., Skaug, B., Jiang, Q.X., and Chen, Z.J. (2011). MAVS forms functional prion-like aggregates to activate and propagate antiviral innate immune response. Cell *146*, 448-461.

Jiang, X., Kinch, L.N., Brautigam, C.A., Chen, X., Du, F., Grishin, N.V., and Chen, Z.J. (2012). Ubiquitin-induced oligomerization of the RNA sensors RIG-I and MDA5 activates antiviral innate immune response. Immunity *36*, 959-973.

Jones, J.W., Kayagaki, N., Broz, P., Henry, T., Newton, K., O'Rourke, K., Chan, S., Dong, J., Qu, Y., Roose-Girma, M.*, et al.* (2010). Absent in melanoma 2 is required for innate immune recognition of Francisella tularensis. Proc Natl Acad Sci U S A *107*, 9771-9776.

Jucker, M., and Walker, L.C. (2013). Self-propagation of pathogenic protein aggregates in neurodegenerative diseases. Nature *501*, 45-51.

Kushnirov, V.V. (2000). Rapid and reliable protein extraction from yeast. Yeast *16*, 857-860.

Li, J., McQuade, T., Siemer, A.B., Napetschnig, J., Moriwaki, K., Hsiao, Y.S., Damko, E., Moquin, D., Walz, T., McDermott, A.*, et al.* (2012). The RIP1/RIP3 necrosome forms a functional amyloid signaling complex required for programmed necrosis. Cell *150*, 339-350.

Liebman, S.W., and Chernoff, Y.O. (2012). Prions in yeast. Genetics *191*, 1041-1072.

Liepinsh, E., Barbals, R., Dahl, E., Sharipo, A., Staub, E., and Otting, G. (2003). The death-domain fold of the ASC PYRIN domain, presenting a basis for PYRIN/PYRIN recognition. J Mol Biol *332*, 1155-1163.

Lin, S.C., Lo, Y.C., and Wu, H. (2010). Helical assembly in the MyD88-IRAK4-IRAK2 complex in TLR/IL-1R signalling. Nature *465*, 885-890.

Liu, S., Chen, J., Cai, X., Wu, J., Chen, X., Wu, Y.T., Sun, L., and Chen, Z.J. (2013). MAVS recruits multiple ubiquitin E3 ligases to activate antiviral signaling cascades. Elife *2*, e00785.

Majumdar, A., Cesario, W.C., White-Grindley, E., Jiang, H., Ren, F., Khan, M.R., Li, L., Choi, E.M., Kannan, K., Guo, F.*, et al.* (2012a). Critical role of amyloid-like oligomers of Drosophila Orb2 in the persistence of memory. Cell *148*, 515-529.

Majumdar, A., Cesario, W.C., White-Grindley, E., Jiang, H., Ren, F., Khan, M.R., Li, L., Choi, E.M., Kannan, K., Guo, F.*, et al.* (2012b). Critical Role of Amyloid-like Oligomers of Drosophila Orb2 in the Persistence of Memory. Cell.

Martinon, F., Burns, K., and Tschopp, J. (2002). The inflammasome: a molecular platform triggering activation of inflammatory caspases and processing of proIL-beta. Mol Cell *10*, 417-426.

Medzhitov, R. (2010). Innate immunity: quo vadis? Nat Immunol *11*, 551-553.

Medzhitov, R., Shevach, E.M., Trinchieri, G., Mellor, A.L., Munn, D.H., Gordon, S., Libby, P., Hansson, G.K., Shortman, K., Dong, C.*, et al.* (2011). Highlights of 10 years of immunology in Nature Reviews Immunology. Nat Rev Immunol *11*, 693-702.

Moresco, E.M., Vine, D.L., and Beutler, B. (2011). Prion-like behavior of MAVS in RIG-I signaling. Cell Res.

Ness, F., Ferreira, P., Cox, B.S., and Tuite, M.F. (2002). Guanidine hydrochloride inhibits the generation of prion "seeds" but not prion protein aggregation in yeast. Mol Cell Biol *22*, 5593-5605.

Osherovich, L.Z., Cox, B.S., Tuite, M.F., and Weissman, J.S. (2004). Dissection and design of yeast prions. PLoS Biol *2*, E86.

Parham, S.N., Resende, C.G., and Tuite, M.F. (2001). Oligopeptide repeats in the yeast protein Sup35p stabilize intermolecular prion interactions. Embo J *20*, 2111-2119.

Park, H.H., Lo, Y.C., Lin, S.C., Wang, L., Yang, J.K., and Wu, H. (2007a). The death domain superfamily in intracellular signaling of apoptosis and inflammation. Annu Rev Immunol *25*, 561-586.

Park, H.H., Logette, E., Raunser, S., Cuenin, S., Walz, T., Tschopp, J., and Wu, H. (2007b). Death domain assembly mechanism revealed by crystal structure of the oligomeric PIDDosome core complex. Cell *128*, 533-546.

Potter, J.A., Randall, R.E., and Taylor, G.L. (2008). Crystal structure of human IPS-1/MAVS/VISA/Cardif caspase activation recruitment domain. BMC Struct Biol *8*, 11.

Prusiner, S.B. (1982). Novel proteinaceous infectious particles cause scrapie. Science *216*, 136-144.

Prusiner, S.B. (1998). Prions. Proc Natl Acad Sci U S A *95*, 13363-13383.

Qiao, Q., Yang, C., Zheng, C., Fontan, L., David, L., Yu, X., Bracken, C., Rosen, M., Melnick, A., Egelman, E.H.*, et al.* (2013). Structural architecture of the

CARMA1/Bcl10/MALT1 signalosome: nucleation-induced filamentous assembly. Mol Cell *51*, 766-779.

Ramaswami, M., Taylor, J.P., and Parker, R. (2013). Altered Ribostasis: RNA-Protein Granules in Degenerative Disorders. Cell *154*, 727-736.

Ren, P.H., Lauckner, J.E., Kachirskaia, I., Heuser, J.E., Melki, R., and Kopito, R.R. (2009). Cytoplasmic penetration and persistent infection of mammalian cells by polyglutamine aggregates. Nat Cell Biol *11*, 219-225.

Saupe, S.J. (2011). The [Het-s] prion of Podospora anserina and its role in heterokaryon incompatibility. Semin Cell Dev Biol *22*, 460-468.

Schroder, K., and Tschopp, J. (2010). The inflammasomes. Cell *140*, 821-832.

Serio, T.R., Cashikar, A.G., Kowal, A.S., Sawicki, G.J., Moslehi, J.J., Serpell, L., Arnsdorf, M.F., and Lindquist, S.L. (2000). Nucleated conformational conversion and the replication of conformational information by a prion determinant. Science *289*, 1317-1321.

Seth, R.B., Sun, L., Ea, C.K., and Chen, Z.J. (2005). Identification and characterization of MAVS, a mitochondrial antiviral signaling protein that activates NF-kappaB and IRF 3. Cell *122*, 669-682.

Seuring, C., Greenwald, J., Wasmer, C., Wepf, R., Saupe, S.J., Meier, B.H., and Riek, R. (2012). The mechanism of toxicity in HET-S/HET-s prion incompatibility. PLoS Biol *10*, e1001451.

Shorter, J., and Lindquist, S. (2005). Prions as adaptive conduits of memory and inheritance. Nat Rev Genet *6*, 435-450.

Si, K., Choi, Y.B., White-Grindley, E., Majumdar, A., and Kandel, E.R. (2010). Aplysia CPEB can form prion-like multimers in sensory neurons that contribute to long-term facilitation. Cell *140*, 421-435.

Si, K., Giustetto, M., Etkin, A., Hsu, R., Janisiewicz, A.M., Miniaci, M.C., Kim, J.H., Zhu, H., and Kandel, E.R. (2003). A neuronal isoform of CPEB regulates local protein synthesis and stabilizes synapse-specific long-term facilitation in aplysia. Cell *115*, 893-904.

Sondheimer, N., and Lindquist, S. (2000). Rnq1: an epigenetic modifier of protein function in yeast. Mol Cell *5*, 163-172.

Subramanian, N., Natarajan, K., Clatworthy, M.R., Wang, Z., and Germain, R.N. (2013). The adaptor MAVS promotes NLRP3 mitochondrial localization and inflammasome activation. Cell *153*, 348-361.

Sun, L., Deng, L., Ea, C.K., Xia, Z.P., and Chen, Z.J. (2004). The TRAF6 ubiquitin ligase and TAK1 kinase mediate IKK activation by BCL10 and MALT1 in T lymphocytes. Mol Cell *14*, 289-301.

Sun, L., Wu, J., Du, F., Chen, X., and Chen, Z.J. (2013). Cyclic GMP-AMP synthase is a cytosolic DNA sensor that activates the type I interferon pathway. Science *339*, 786-791.

Suzuki, G., Shimazu, N., and Tanaka, M. (2012). A yeast prion, Mod5, promotes acquired drug resistance and cell survival under environmental stress. Science *336*, 355-359.

Takeuchi, O., and Akira, S. (2010). Pattern recognition receptors and inflammation. Cell *140*, 805-820.

Tanaka, Y., and Chen, Z.J. (2012). STING specifies IRF3 phosphorylation by TBK1 in the cytosolic DNA signaling pathway. Sci Signal *5*, ra20.

Tijsterman, M., and Plasterk, R.H. (2004). Dicers at RISC; the mechanism of RNAi. Cell *117*, 1-3.

Toyama, B.H., and Weissman, J.S. (2011). Amyloid structure: conformational diversity and consequences. Annu Rev Biochem *80*, 557-585.

True, H.L., and Lindquist, S.L. (2000). A yeast prion provides a mechanism for genetic variation and phenotypic diversity. Nature *407*, 477-483.

Tuite, M.F., and Serio, T.R. (2010). The prion hypothesis: from biological anomaly to basic regulatory mechanism. Nat Rev Mol Cell Biol *11*, 823-833.

Vajjhala, P.R., Mirams, R.E., and Hill, J.M. (2012). Multiple binding sites on the pyrin domain of ASC protein allow self-association and interaction with NLRP3 protein. J Biol Chem *287*, 41732-41743.

von Bernuth, H., Picard, C., Jin, Z., Pankla, R., Xiao, H., Ku, C.L., Chrabieh, M., Mustapha, I.B., Ghandil, P., Camcioglu, Y.*, et al.* (2008). Pyogenic bacterial infections in humans with MyD88 deficiency. Science *321*, 691-696.

Wickner, R.B. (1994). [URE3] as an altered URE2 protein: evidence for a prion analog in Saccharomyces cerevisiae. Science *264*, 566-569.

Wu, J., Sun, L., Chen, X., Du, F., Shi, H., Chen, C., and Chen, Z.J. (2013). Cyclic GMP-AMP is an endogenous second messenger in innate immune signaling by cytosolic DNA. Science *339*, 826-830.

Yoneyama, M., Kikuchi, M., Natsukawa, T., Shinobu, N., Imaizumi, T., Miyagishi, M., Taira, K., Akira, S., and Fujita, T. (2004). The RNA helicase RIG-I has an essential function in double-stranded RNA-induced innate antiviral responses. Nat Immunol *5*, 730-737.

Zeng, W., Sun, L., Jiang, X., Chen, X., Hou, F., Adhikari, A., Xu, M., and Chen, Z.J. (2010). Reconstitution of the RIG-I pathway reveals a signaling role of unanchored polyubiquitin chains in innate immunity. Cell *141*, 315-330.

Zeng, W., Xu, M., Liu, S., Sun, L., and Chen, Z.J. (2009). Key role of Ubc5 and lysine-63 polyubiquitination in viral activation of IRF3. Mol Cell *36*, 315-325.

Zhang, X., Shi, H., Wu, J., Sun, L., Chen, C., and Chen, Z.J. (2013). Cyclic GMP-AMP Containing Mixed Phosphodiester Linkages Is An Endogenous High-Affinity Ligand for STING. Mol Cell *51*, 226-235.